Jurnal Penelitian dan Pengkajian Ilmu Pendidikan: e-Saintika
https://journal-center.litpam.com/index.php/e-Saintika/index

July 2021 Vol. 5, No. 2
e-ISSN: 2615-6881
pp. 182-194

Synthesis and Characterization of ZnO Thin Layers using Sol-Gel Spin Coating Method

[1]Sukainil Ahzan, [2]Darminto, [3]Ferry Anggoro Ardy Nugroho, [*1]Saiful Prayogi
[1]Faculty of Applied Science and Engineering, Universitas Pendidikan Mandalika, Jl. Pemuda No. 59A, Mataram 83126, Indonesia.
[2]Faculty of Mathematics and Science, Institut Teknologi Sepuluh Nopember (ITS), Jl. Raya ITS, Surabaya 60111, Indonesia.
[2]Departmet of Physics and Astronomy, Vrije Universiteit Amsterdam, De Boelelaan 1081, 1081 HV Amsterdam, The Netherlands.

*Corresponding Author e-mail: saifulprayogi@ikipmataram.ac.id

Received: May 2021; Revised: June 2021; Published: July 2021

Abstract

The potential of thin layer in many applications has led to research on the development of many new materials and their fabrication methods. This study aimed to synthesize a thin layer of ZnO using the facile and low-cost sol-gel spin coating method. The ZnO thin layer is deposited on a glass substrate and analyzed to observe the influence of the deposition variables such as heating and rotation speed, and its aging. The characterization methods include the identification of the formed phase using X-Ray Diffractometer (XRD), and the microstructure and elemental composition using Scanning Electron Microscopy (SEM) coupled with EDS (Energy Dispersive Spectrometer). The study shows that a thin layer of ZnO is successfully deposited on a glass substrate by heat treatment at temperatures of 300 °C and 500 °C. Furthermore, XRD reveals that higher heating temperatures result in higher diffraction peak intensity. At a heating temperature of 300 °C crystals are formed but are not yet perfectly oriented, while they are at 500 °C. On the other hand, higher spin coating rotation speed gives rise to lower intensity of diffraction peak. The ZnO crystallization is easier to form in the coating process with a lower rotation (1500 rpm). Interestingly, the thin layer is stable over time where there is no significant change in each sample, both in terms of intensity and width of the ZnO crystal peak. The results indicate that gel precursor aged less than two days can form ZnO crystals. Finally, SEM results show that the surface morphology of the ZnO layer heated at 500 °C has an average grain size of 300 nm. Based on the cross-sectional results of SEM shows that the higher the coating rotation speed has resulted the thinner of the ZnO layer, where the thickness of the resulting layer is on order >5 μm.

Keywords: synthesis; characterization; ZnO thin layer; sol-gel spin coating

How to Cite: Ahzan, S., Darminto, D., Nugroho, F. A. A., & Prayogi, S. (2021). Synthesis and Characterization of ZnO Thin Layers using Sol-Gel Spin Coating Method. *Jurnal Penelitian Dan Pengkajian Ilmu Pendidikan: E-Saintika*, *5*(2), 182-194. https://doi.org/10.36312/esaintika.v5i2.506

https://doi.org/10.36312/esaintika.v5i2.506

INTRODUCTION

In recent decades, as the demand for energy continues to increase, there has been tremendous interest in developing renewable energy sources and environmentally friendly technological device systems (Matsuda & Kawamura, 2016), some of which include fuel-cells, solar-cells, supercapacitors, and efficient batteries (Tan et al., 2021). In accordance with the interest in many fields of application, thin layers of several materials have been developed by the sol-gel method (Soo et al., 2013a, 2013b). Since

being introduced by Groove in 1852, thin layer technology has undergone many developments in terms of manufacturing methods, materials used, and applications (Greene, 2017). In the thin layer processing technique, the material commonly used is metal (Jittiarporn et al., 2017; Mironyuk et al., 2020; Shi et al., 2020; Tan et al., 2020), organic, inorganic, and hybrid organic-inorganic (Kawamura et al., 2010; Nisticò et al., 2017; Takahashi, 2018; Takahashi et al., 2014).

The advancement of thin films by the sol-gel method for various applications is highly dependent on the material used. In fuel-cell applications, for example, PDDA films and microparticles of $PhSiO_{3/2}$ succeeded in increasing proton conductivity to achieve a stable proton supply (Daiko et al., 2008). Likewise, Pt/TiO_2 was demonstrated as an electrocatalyst for fuel-cell electrolyte membrane applications (Nbelayim et al., 2020). The performance of a lightweight, high-capacity battery is developed from the synthesis of Li/Ti double alkoxides in a $Li_4Ti_5O_{12}$ thin film (Mosa & Aparicio, 2020), and LiF/FeF_2 in the form of $Li0.5FeF_3$ (Kim et al., 2012; Tawa et al., 2019). Formation of superhydrophobic/superhydrophilic layers in film fabrication including surface design and film coating using Al_2O_3, ZrO_2, and TiO_2 materials (Tadanaga et al., 2004). In addition, the development of thin films by the sol-gel method is used in the extraction technology of waste disposal, especially heavy metal adsorbents , such as electro-spinned flexible Fe_3O_4 fibers (Shi et al., 2020) and yttria-stabilized ZrO_2 membranes (Qin et al., 2020). The most extensively researched is the application of thin layers as solar-cells (dye-sensitized solar cells, DSSC) (Abd-Ellah et al., 2016; Nbelayim et al., 2017, 2018, 2020; Tan et al., 2017; Toe et al., 2020), from zinc oxide material (ZnO) (Khan et al., 2017; Muchuweni et al., 2017; Prasada Rao et al., 2010).

Sol-gel coating techniques commonly used include spray coating, dip coating, roll coating, and spin coating (Tan et al., 2021). Among these, spin-coating method is the most frequently used (Khan et al., 2017). This method combines simple physical and chemical methods and has several advantages compared to other methods, for instance being cost-efficient with relatively simple setup, and excellent control over the thickness (through parameters of time, rotational speed, and viscosity of the solution) and the homogeneity of the layer (Cheng et al., 2003).

Among thin film-forming materials, zinc oxide (ZnO) is the most extensively studied because it is one of the transparent semi-conductive oxides (Zou et al., 2007) with a relatively high exciton binding energy (60 mEV) and a wide band gap around of 3.2 to 3.4 eV (Rwenyagila et al., 2014; Sivaramakrishnan & Alford, 2010; Valverde-Aguilar & Manríquez Zepeda, 2015). These advantages of optical and electrical properties allow ZnO to be applied as optical waveguides, optoelectronic devices (Çopuroğlu et al., 2009; Khan et al., 2017; Rwenyagila et al., 2014), piezoelectricity, conductive gas sensors, transparent conductive electrodes, photocatalysts and DSSC (Djurišić et al., 2010). One of the exciting properties of ZnO is its crystal formation process that occurs at temperatures under 400 ^oC. This phenomenon depends on the type of deposition and the solvent used. Previous studies showed that crystalline ZnO was formed using ethylene glycol and glycerol as a solvent at a heating temperature of 200 ^oC (Torres Delgado et al., 2009). Heating at temperatures below 300^oC is an early stage of heating, where the crystal structure has been formed but has not been oriented perfectly. Furthermore, with higher heating at 400 ^oC and 500 ^oC, the ZnO crystal structure will be perfectly oriented (Raoufi & Raoufi, 2009). Another attractive property of ZnO to observe is aging. Aging is the storage of sol-gel for a certain time

before being used as a coating material. The aging process affects the physical, electrical, and optical properties of the ZnO thin film (Xu et al., 2009).

Literature surveys reveal that reports on the properties of ZnO thin films deposited by the sol-gel technique is lacking (Khan et al., 2017). Here, we develop a thin layer of ZnO material by the sol-gel spin coating method and assess its crystallization properties and morphology. The variables that are the focus of this study include heat treatment, rotation speed, and aging

METHOD

A thin layer was deposited on a glass substrate of 5 x 10 mm^2 using a sol-gel method using zinc acetate dehydrate {$Zn(CH_3COO)_2.2H_2O$} powder (M: 219.49 g/mol, 99% Merck, Germany) with a molar ratio of 1:1 MEA:ZnAc. Ethanol (C_2H_6O) (99% technical, Merck) was used as solvent and ethanolamine (MEA: C_2H_7NO) as stabilizer, each with a purity of 99%. The solution was prepared by magnetic stirring at ±70 °C for 30 minutes. ZnAc was rather difficult to dissolve in ethanol. Therefore the dissolution process must be accompanied by heating, which was carried out on a hot plate with a temperature range of 80 to 100 °C. This was followed by the addition of MEA. After the heating process for 30 to 40 minutes, the solution was then allowed to stand at room temperature to form a gel. The gel was the divided into five parts and each was aged for 0, 10, 24, 48 and 72 hours, in air with a temperature of ±25°C and humidity of 70±5%.

The thermal behavior of ZnO gel was tested using Differential Thermal Analysis (DTA) and Thermogravimetric Analysis (TGA). This analysis aimed to observe changes in energy and mass as function of temperature. The DTA/TGA analysis results are used as a reference in determining the temperature at which the phase transformation occurs.

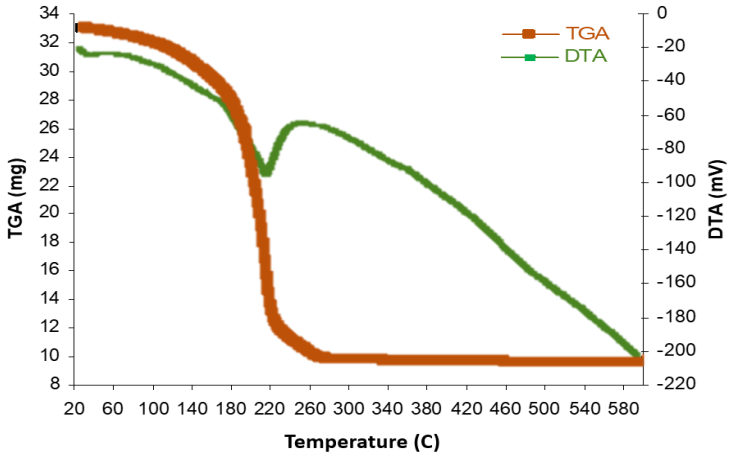

Figure 1. DTA-TGA test results of ZnO thin film deposited by spin coat sol-gel.

Based on the results of the TGA (Fig. 1), it can be seen that there is 90% decrease in mass up to a temperature of 280 °C, after which there is no further decrease in mass. This decrease in mass is followed by energy release or endothermic (DTA Graph in Fig. 1). Based on the DTA and TGA graphs, it is estimated that the change of ZnO + H_2O into ZnO crystals occurs on heating above 280 °C, so that the ZnO layer pre-heating process can be carried out at a temperature of 300 °C.

The deposition of the thin layer on a glass substrate with spin coating was also carried out at 1500, 2000, and 2500 rpm variations. A thin layer of ZnO was heated

using a furnace. The heating process was carried out in 3 stages. The first heating for 1 hour at a temperature of 100 °C (calcination) aimed to gradually remove the water content and residual solvent in the layer. The second heating at 300 °C, where the temperature was slowly increased from room temperature to 300 °C for 5 hours, was held for 6 minutes. This stage was a pre-heating stage that functioned to remove solvents from ethanol, water, MEA, and facilitated ZnOH conversion to ZnO. The next stage was post-heating or final heating at a temperature of 500 °C. Like the pre-heating process, the temperature rise was set slowly from room temperature to 500 °C in 10 hours, then held for 10 minutes. This post-heating functioned to form ZnO particles with uniform crystal orientation and eliminate the pores.

The characterization of the coating results included identification of the formed phase using X-ray Diffractometer (XRD) with the help of a search match and refinement program using Rietica software with the comparison is standard data (CPI ZnO 1011259), layer microstructure, and elemental composition observed by Scanning Electron Microscopy (SEM) coupled with EDS (Energy Dispersive Spectrometer).

RESULTS AND DISCUSSION

Effect of heating on the ZnO crystal layer

The X-ray diffraction pattern of the ZnO layer deposited at 2000 rpm at various heating temperature and aged for 24 hours is shown in Figure 2.

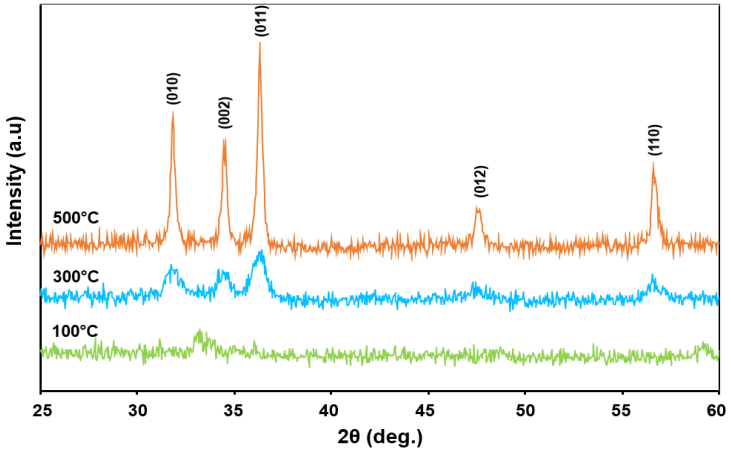

Figure 2. XRD pattern of ZnO layer with the variation of heating temperature

Based on Figure 2, it can be seen that the layer heated at a temperature of 100 °C forms two peaks at an angle of 33.15° and 59.30°. These peaks correspond to zinc propianate ($C_6H_{10}O_4Zn$) phase and zinc salicylate dihydrete {($C_6H_{10}O_6Zn$).$2H_2O$} phase, respectively. These peaks clearly originate from the solvents on the layer.

At a heating temperature of 300 °C crystals are formed but are not yet perfectly oriented. At 500 °C, the ZnO crystals are perfectly oriented. This is consistent with the results of DTA-TGA (cf. Fig. 1) in that the formation of ZnO occurs above 280 °C. With the help of the Rietica program, hexagonal ZnO has been formed with lattice parameters for a temperature of 300 °C (a = 3,245 Å, c = 5,209 Å) and a temperature of 500°C (a = 3,249 Å, c = 5,205 Å). In the range of 2θ of 25° to 60°, crystal plane peaks are formed, indicating that the layer obtained is polycrystalline.

Pre- and post-heating affect the ZnO layer in the form of solvent evaporation and reaction material decomposition. At low pre-heating temperature (< 300 °C), the (100), (002), and (101) diffraction peaks appeared with random preferential growth. This

happens because at this temperature, the reagents have completely evaporated, and the thermal decomposition of the precursors has not yet occurred. Still, they occur at post-heating temperatures above 500 °C (Suwanboon et al., 2008). The increase in the intensity of the diffraction peak at higher temperatures is due to greater energy available to increase the movement of atoms, which increases the quality and crystallization of the layer (Mandal et al., 2008).

Effect of spin coating speed on ZnO layer

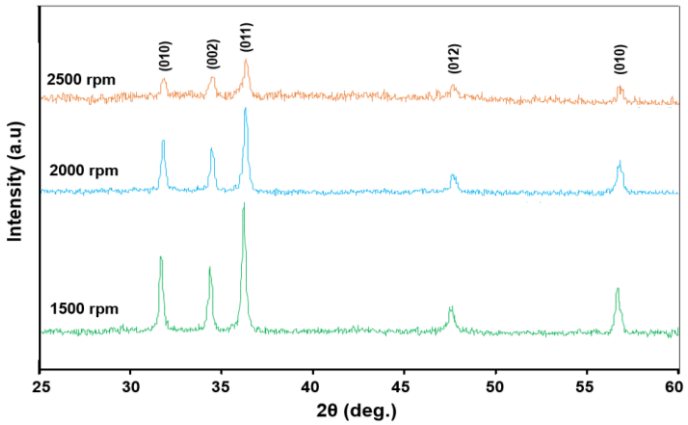

Figure 3. The XRD pattern of the ZnO layer with variations in spin coat rotational speed.

Figure 3 shows XRD results for ZnO layers made with variations in rotational speed of 1500, 2000, and 2500 rpm. The XRD peaks of the three samples show a decrease in intensity as rotation speed increases. This happens because ZnO crystallization is easier to form in the coating process with a lower rotation (1500 rpm).

Effect of aging on ZnO crystal layer

The XRD pattern of the synthesized ZnO layer with variations in aging of the precursor gel is presented in Figure 4.

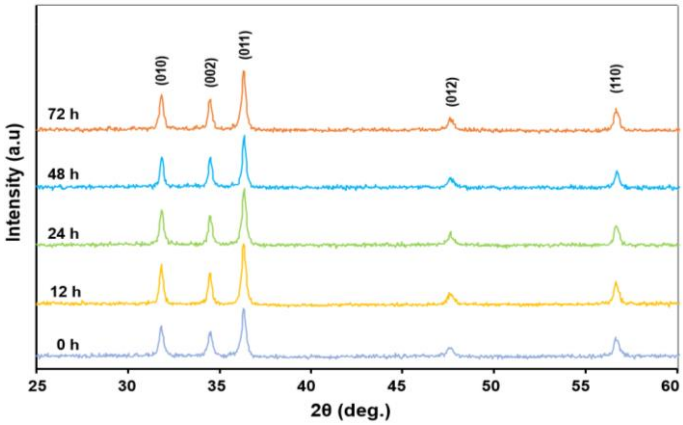

Figure 4. XRD pattern of deposited ZnO layer with an aging variation.

Based on Figure 4, there is no significant change in each sample, both in terms of intensity and width of the ZnO crystal peak. These results indicate that gel precursor aged less than two days can form ZnO crystals. The results of another study reported that after aging for seven days, the peak intensity (002) of ZnO increased compared to samples aged for up to two days (Maldonado et al., 2010). This may occur because

aging can cause further condensation of active groups and ZnO aggregation in solution and cause significant growth at peak intensity (002) of ZnO (Fathollahi & Amini, 2001).

Surface morphology of ZnO thin layer

SEM photos of the ZnO layer surface heated at 100, 300, and 500 °C, respectively, are presented in Figure 5.

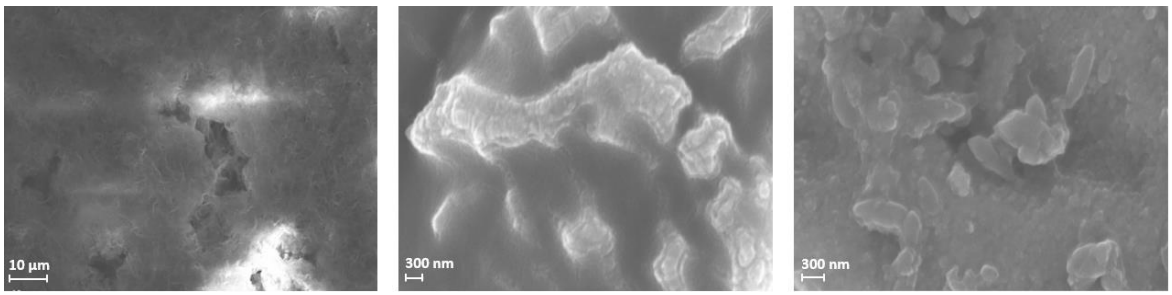

(a) (b) (c)

Figure 5. SEM photos of the ZnO layer surface heated at: (a) 100°C, (b) 300°C, and (c) 500°C.

At a temperature of 100°C (Fig. 5a), the layer is still coarse and porous, with a pore size of approximately 6–8 µm. This is because the layer still contains water molecules and solvents that have not completely evaporated at this temperature. When the layer is heated at 300 °C (pre-heating), the remaining organic matter can evaporate completely, and ZnO grains begin to grow (Fig. 5b), but the distance between the particles is still relatively large. When the ZnO layer is heated at 500 °C (Fig. 5c), the atoms in the existing grains receive sufficient driving force energy to diffuse to form new, larger grains. As a result of this inter-grain diffusion, necking will be formed, resulting in the shrinking of the boundary between grains and porosity (Fig. 5c). The average grain size at this temperature is about 300 nm.

To this end, the morphology and crystal structure of the ZnO layer made by the sol-gel process is influenced by the solvent, pre-heating and post-heating temperatures, sol concentration, substrate, and coating process (Habibi & Khaledi Sardashti, 2008). The ZnO layer's nucleation thermodynamics and crystal growth showed a transformation from an amorphous to crystalline state. The growth of crystals with the dominant c-axis orientation depends on the surface energy of the layer and the glass substrate and the interfacial energy between them. In crystal growth, the growing fields depend on the loss of slow-growing fields, with lower surface energies.

In addition to heat treatment, the morphology and thickness of the ZnO layer are also affected by the spin coating speed. Figure 6 shows the surface morphology of the coated layer at 1500, 2000, and 2500 rpm.

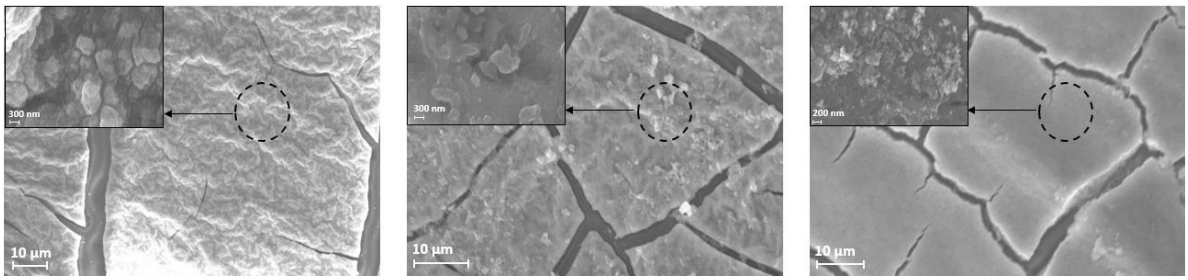

(a) (b) (c)

Figure 6. SEM photos of the ZnO layer surface coated with variations in rotation speed: (a) 1500 rpm, (b) 2000 rpm, and (c) 2500 rpm.

Based on Figure 6, it can be seen that the higher the rotation speed, the smoother the coating obtained, with smaller average grain size. The ZnO layer coated at 1500 and 2000 rpm has similar average grain size of 300 nm, while the ZnO layer coated at 2500 rpm has an average grain size of 100 nm. The results are consistent with previous studies that reported that the higher the rotational speed used to make the ZnO layer, the smaller of grain size produced (Ilican et al., 2008). The cross-sectional analysis of the coated ZnO layer with variations in rotational speed is presented in Figure 7.

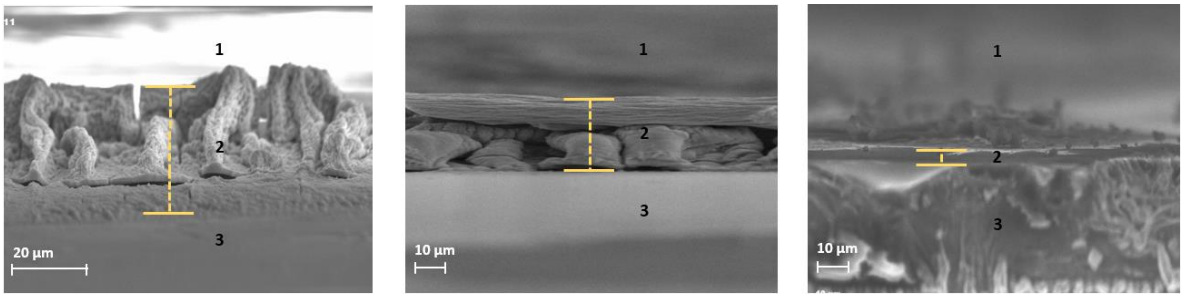

(a) (b) (c)

Figure 7. Cross-section of the coated ZnO layer with variations in rotational speed: (a) 1500 rpm, (b) 2000 rpm, and (c) 2500 rpm. (1 = air, 2 = ZnO layer thickness, 3 = substrate)

The results show that the thickness of the ZnO layer coated with 1500 rpm rotation is about 30 µm (Fig. 7a), while the layer coated with 2000 rpm rotation is about 20 µm (Fig. 7b), 2500 rpm at about 5 µm (Fig. 7c). Therefore it is confirmed that the thickness of the ZnO layer gets thinner as the rotation speed increases. In forming a coating on the substrate, it takes a large enough centrifugal speed to distribute the gel over the entire surface and remove the excess gel to the outside of the substrate. If the rotational speed is increased, the previously attached gel will be thrown out of the substrate, and the layer will thin out, or it can also disappear. This is because the binding force between the substrate and the gel is not strong enough to withstand the centrifugal force, which is too high. So, the faster the coating rotation, the more gel will leave the substrate so that the resulting layer is thinner.

From the results in Figure 6, although the layer looks smooth, most of the areas in the layer have many micron-sized cracks. These cracks are caused by the uneven heating rate on the surface of the coating layer and the different thermal coefficient between the substrate and the coating layer. Cracks also occur in the area between the

layer and the substrate (Fig. 6). Based on the cross-sectional photo of the ZnO layer (Fig. 7), it can be seen that the layer is not completely attached to the substrate. This condition makes the coating to peel off easily when exposed to scratches or friction from the outside. Cracks can also be seen from the EDX results (see Fig. 8). From the Figure we also see existence of Ca (0.98% wt) in the cracks, that originates from the substrate (from XRF results). Although the Ca content is small, this still indicates that the cracks are intense they penetrate the ZnO layer. Based on the Figure 8, it is estimated that the thickness of the ZnO layer formed with heating at 500 °C is about 5 μm to 20 μm.

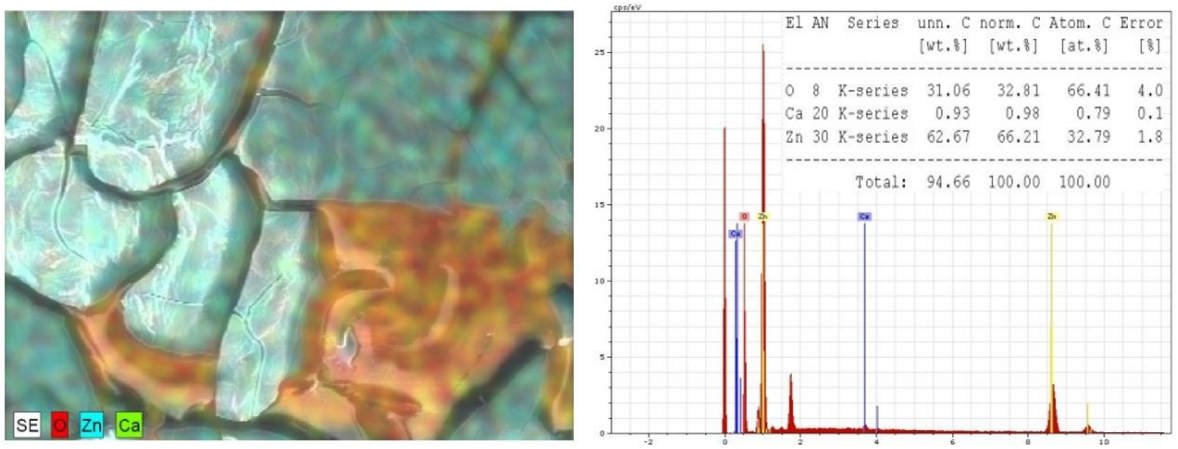

(a) (b)

Figure 8. EDX results of ZnO layer on a glass substrate: (a) surface topography, and (b) elemental content.

Microcracks may occur on the ceramic coating surface with the cracks spreading along the grain boundaries (Sakka, 2018). This phenomena happens because the layer and the substrate have a huge difference in the coefficient of thermal expansion. The spread of microcracks along the grain boundaries is formed before the crystallization process. These microcracks can be prevented by equalizing the coefficient of thermal expansion (α) between the coating and the substrate. For example BaTiO3 (α =140 x 10^{-7} K^{-1}), the layer has microcracks when deposited on a SiO2 glass substrate (α = 5 x 10^{-7} K^{-1}), but BaTiO3 has no microcracks on a single crystal substrate of MgO (α = 135 x 10^{-7} K^{-1}) (Sakka, 2018). Microcracks can occur during the heating process at low temperatures (100°C - 400°C). In another study (Kozuka & Hirano, 2000) reported that in the production of the titania layer, the crystal structure appears at a temperature of 500°C, while cracks appear at temperatures below it. This means that the crack occurs before the crystallization process.

Microcracks can also occur due to variations in the thickness of the gel layer. In the titania layer made with variations in thickness, the thicker layer is obtained, which tends to crack at low temperatures (Kozuka & Hirano, 2000). This happens because the thickness affects the occurrence of intrinsic stress during the heating process. The crack formation also depends on the heating rate. Cracks appear at higher temperatures when the coating is heated at a low heating rate. At low heating, the rate will produce a smaller porosity. This indicates that the low heating rate allows sufficient time for the coating to solidify during heating resulting in high tensile stresses in the substrate plane.

CONCLUSION

The ZnO layer was successfully deposited on a glass substrate by heat treatment at 300 °C and 500 °C. At a heating temperature of 100°C, the ZnO structure has not yet been formed, and when the heating temperature is 300 °C, crystals have started to form but have not been oriented perfectly. ZnO crystals are perfectly oriented at 500 °C. XRD results show that the higher heating temperature has resulted in higher diffraction peak intensity. At a heating temperature of 300 °C crystals are formed but are not yet perfectly oriented while at 500 °C they are. On the other hand, higher spin coating rotation speed gives rise to lower intensity of diffraction peak. The ZnO crystallization is easier to form in the coating process with a lower rotation (1500 rpm). Interestingly, the thin layer is stable over time where there is no significant change in each sample, both in terms of intensity and width of the ZnO crystal peak. The results indicate that gel precursor aged less than two days can form ZnO crystals. SEM results show that the surface morphology of the ZnO layer heated at 500 °C has an average grain size of 300 nm. The cross-sectional results of SEM show that the higher the rotation speed, the thinner the resulting ZnO layer, where the thickness of the resulting layer is on the order of > 5 μm.

RECOMMENDATION

The XRD results of the ZnO layer deposited on the glass substrate were all polycrystalline in structure. Efforts to make ZnO layer single crystal must be continued, by proper selection of substrate and higher post-heating. In addition, the SEM results show that the surface morphology of the ZnO layer is not homogeneous, there are many cracks and the size is still thick. For this reason, it is necessary to carry out more in-depth experiments in terms of the use of appropriate concentrations, speeds, and rotation times, as well as the selection of a substrate that has a heat capacity and plane orientation in accordance with the ZnO layer, for example alumina ceramic material.

ACKNOWLEDGMENT

This research received no specific grant from any funding agency in the public, commercial, or not for profit sectors.

REFERENCES

Abd-Ellah, M., Moghimi, N., Zhang, L., Thomas, Joseph. P., McGillivray, D., Srivastava, S., & Leung, K. T. (2016). Plasmonic gold nanoparticles for ZnO-nanotube photoanodes in dye-sensitized solar cell application. *Nanoscale*, *8*(3), 1658–1664. https://doi.org/10.1039/C5NR08029K

Cheng, Z., Zhang, J., & Kronmüller, H. (2003). Magnetically soft phase in magnetization reversal processes of nanocomposite Sm 2 Fe 15 Ga 2 C x / α − Fe permanent magnetic materials. *Physical Review B*, *68*(14), 144417. https://doi.org/10.1103/PhysRevB.68.144417

Çopuroğlu, M., Koh, L. H. K., O'Brien, S., & Crean, G. M. (2009). Comparative characterisation of zinc oxide thin films prepared from zinc acetate with or without water of hydration via the sol–gel method. *Journal of Sol-Gel Science and Technology*, *52*(3), 432–438. https://doi.org/10.1007/s10971-009-2016-0

Daiko, Y., Sakamoto, H., Katagiri, K., Muto, H., Sakai, M., & Matsuda, A. (2008). Deposition of Ultrathin Nafion Layers on Sol–Gel-Derived Phenylsilsesquioxane

Particles via Layer-by-Layer Assembly. *Journal of The Electrochemical Society*, *155*(5), B479. https://doi.org/10.1149/1.2885101

Djurišić, A. B., Ng, A. M. C., & Chen, X. Y. (2010). ZnO nanostructures for optoelectronics: Material properties and device applications. *Progress in Quantum Electronics*, *34*(4), 191–259. https://doi.org/10.1016/j.pquantelec.2010.04.001

Fathollahi, V., & Amini, M. M. (2001). Sol–gel preparation of highly oriented gallium-doped zinc oxide thin films. *Materials Letters*, *50*(4), 235–239. https://doi.org/10.1016/S0167-577X(01)00231-2

Greene, J. E. (2017). Review Article: Tracing the recorded history of thin-film sputter deposition: From the 1800s to 2017. *Journal of Vacuum Science & Technology A: Vacuum, Surfaces, and Films*, *35*(5), 05C204. https://doi.org/10.1116/1.4998940

Habibi, M. H., & Khaledi Sardashti, M. (2008). Structure and morphology of nanostructured zinc oxide thin films Prepared by dip-vs. Spin-coating methods. *Journal of the Iranian Chemical Society*, *5*(4), 603–609. https://doi.org/10.1007/BF03246140

Ilican, S., Caglar, Y., & Caglar, M. (2008). Preparation and Characterization Of ZnO Thin Films Deposited By Sol-Gel Spin Coating Method. *Journal of Optoelectronics and Advanced Materials*, *10*(10), 2578–2583.

Jittiarporn, P., Badilescu, S., Al Sawafta, M. N., Sikong, L., & Truong, V.-V. (2017). Electrochromic properties of sol–gel prepared hybrid transition metal oxides – A short review. *Journal of Science: Advanced Materials and Devices*, *2*(3), 286–300. https://doi.org/10.1016/j.jsamd.2017.08.005

Kawamura, G., Sato, S., Muto, H., Sakai, M., Lim, P. B., Watanabe, K., Inoue, M., & Matsuda, A. (2010). AgBr nanocrystal-dispersed silsesquioxane–titania hybrid films for holographic materials. *Materials Letters*, *64*(23), 2648–2651. https://doi.org/10.1016/j.matlet.2010.08.068

Khan, M. I., Bhatti, K. A., Qindeel, R., Alonizan, N., & Althobaiti, H. S. (2017). Characterizations of multilayer ZnO thin films deposited by sol-gel spin coating technique. *Results in Physics*, *7*, 651–655. https://doi.org/10.1016/j.rinp.2016.12.029

Kim, S. W., Nam, K. W., Seo, D. H., Hong, J., Kim, K., Gwon, H., & Kang, K. (2012). Energy storage in composites of a redox couple host and a lithium ion host. *Nano Today*, *7*(3), 168–173. https://doi.org/10.1016/j.nantod.2012.04.004

Kozuka, H., & Hirano, M. (2000). Radiative Striations and Surface Roughness of Alkoxide-Derived Spin Coating Films. *Journal of Sol-Gel Science and Technology*, *19*(1/3), 501–504. https://doi.org/10.1023/A:1008772102546

Maldonado, A., Tirado-Guerra, S., Cázares, J. M., & Olvera, M. de la L. (2010). Physical and sensing properties of ZnO:F:Al thin films deposited by sol–gel. *Thin Solid Films*, *518*(7), 1815–1820. https://doi.org/10.1016/j.tsf.2009.09.039

Mandal, S., Goswami, M. L. N., Das, K., Dhar, A., & Ray, S. K. (2008). Temperature dependent photoluminescence characteristics of nanocrystalline ZnO films grown by sol–gel technique. *Thin Solid Films*, *516*(23), 8702–8706. https://doi.org/10.1016/j.tsf.2008.05.016

Matsuda, A., & Kawamura, G. (2016). Sol–Gel Nano-/Micropatterning Process. In L. Klein, M. Aparicio, & A. Jitianu (Eds.), *Handbook of Sol-Gel Science and Technology* (pp. 1–28). Springer International Publishing. https://doi.org/10.1007/978-3-319-19454-7_81-1

Mironyuk, I., Mykytyn, I., Vasylyeva, H., & Savka, K. (2020). Sodium-modified mesoporous TiO2: Sol-gel synthesis, characterization and adsorption activity toward heavy metal cations. *Journal of Molecular Liquids*, *316*, 113840. https://doi.org/10.1016/j.molliq.2020.113840

Mosa, J., & Aparicio, M. (2020). Sol-Gel Synthesis of Nanocrystalline Mesoporous Li4Ti5O12 Thin-Films as Anodes for Li-Ion Microbatteries. *Nanomaterials*, *10*(7), 1369. https://doi.org/10.3390/nano10071369

Muchuweni, E., Sathiaraj, T. S., & Nyakotyo, H. (2017). Synthesis and characterization of zinc oxide thin films for optoelectronic applications. *Heliyon*, *3*(4), e00285. https://doi.org/10.1016/j.heliyon.2017.e00285

Nbelayim, P., Ashida, Y., Maegawa, K., Kawamura, G., Muto, H., & Matsuda, A. (2020). Preparation and Characterization of Stable and Active Pt@TiO $_2$ Core–Shell Nanoparticles as Electrocatalyst for Application in PEMFCs. *ACS Applied Energy Materials*, *3*(4), 3269–3281. https://doi.org/10.1021/acsaem.9b02169

Nbelayim, P., Kawamura, G., Abdel-Galeil, M. M., Tan, W. K., Wei, X., Muto, H., & Matsuda, A. (2018). Effects of multi-sized and -shaped Ag@TiO_2 nanoparticles on the performance of plasmonic dye-sensitized solar cells. *Journal of the Ceramic Society of Japan*, *126*(3), 139–151. https://doi.org/10.2109/jcersj2.17203

Nbelayim, P., Kawamura, G., Kian Tan, W., Muto, H., & Matsuda, A. (2017). Systematic characterization of the effect of Ag@TiO2 nanoparticles on the performance of plasmonic dye-sensitized solar cells. *Scientific Reports*, *7*(1), 15690. https://doi.org/10.1038/s41598-017-15541-z

Nisticò, R., Scalarone, D., & Magnacca, G. (2017). Sol-gel chemistry, templating and spin-coating deposition: A combined approach to control in a simple way the porosity of inorganic thin films/coatings. *Microporous and Mesoporous Materials*, *248*, 18–29. https://doi.org/10.1016/j.micromeso.2017.04.017

Prasada Rao, T., Santhosh Kumar, M. C., Safarulla, A., Ganesan, V., Barman, S. R., & Sanjeeviraja, C. (2010). Physical properties of ZnO thin films deposited at various substrate temperatures using spray pyrolysis. *Physica B: Condensed Matter*, *405*(9), 2226–2231. https://doi.org/10.1016/j.physb.2010.02.016

Qin, H., Guo, W., Huang, X., Gao, P., & Xiao, H. (2020). Preparation of yttria-stabilized ZrO2 nanofiltration membrane by reverse micelles-mediated sol-gel process and its application in pesticide wastewater treatment. *Journal of the European Ceramic Society*, *40*(1), 145–154. https://doi.org/10.1016/j.jeurceramsoc.2019.09.023

Raoufi, D., & Raoufi, T. (2009). The effect of heat treatment on the physical properties of sol–gel derived ZnO thin films. *Applied Surface Science*, *255*(11), 5812–5817. https://doi.org/10.1016/j.apsusc.2009.01.010

Rwenyagila, E. R., Agyei-Tuffour, B., Zebaze Kana, M. G., Akin-Ojo, O., & Soboyejo, W. O. (2014). Optical properties of ZnO/Al/ZnO multilayer films for large area transparent electrodes. *Journal of Materials Research*, *29*(24), 2912–2920. https://doi.org/10.1557/jmr.2014.298

Sakka, S. (2018). Sol-Gel Formation of Bulk Glasses. In L. Klein, M. Aparicio, & A. Jitianu (Eds.), *Handbook of Sol-Gel Science and Technology* (pp. 233–256). Springer International Publishing. https://doi.org/10.1007/978-3-319-32101-1_6

Shi, S., Xu, C., Wang, X., Xie, Y., Wang, Y., Dong, Q., Zhu, L., Zhang, G., & Xu, D. (2020). Electrospinning fabrication of flexible Fe3O4 fibers by sol-gel method with high saturation magnetization for heavy metal adsorption. *Materials & Design*, *186*, 108298. https://doi.org/10.1016/j.matdes.2019.108298

Sivaramakrishnan, K., & Alford, T. L. (2010). Conduction and transmission analysis in gold nanolayers embedded in zinc oxide for flexible electronics. *Applied Physics Letters*, *96*(20), 201109. https://doi.org/10.1063/1.3435467

Soo, M. T., Kawamura, G., Muto, H., Matsuda, A., Lockman, Z., & Cheong, K. Y. (2013a). Design of hierarchically meso–macroporous tetragonal ZrO2 thin films with tunable thickness by spin-coating via sol–gel template route. *Microporous and Mesoporous Materials*, *167*, 198–206. https://doi.org/10.1016/j.micromeso.2012.09.010

Soo, M. T., Kawamura, G., Muto, H., Matsuda, A., Lockman, Z., & Cheong, K. Y. (2013b). Fabrication of well-crystallized mesoporous ZrO2 thin films via Pluronic P123 templated sol–gel route. *Ceramics International*, *39*, S437–S440. https://doi.org/10.1016/j.ceramint.2012.10.109

Suwanboon, S., Tanattha, R., & Tanakorn, R. (2008). Fabrication and properties of nanocrystalline zinc oxide thin film prepared by sol-gel method. *Songklanakarin Journal of Science and Technology*, *30*(1), 65–69.

Tadanaga, K., Fujii, T., Matsuda, A., Minami, T., & Tatsumisago, M. (2004). Micropatterning of Sol-Gel Derived Thin Films Using Hydrophobic-Hydrophilic Patterned Surface. *Journal of Sol-Gel Science and Technology*, *31*(1–3), 299–302. https://doi.org/10.1023/B:JSST.0000048007.43110.fa

Takahashi, M. (2018). Responsive and Adaptive Micro Wrinkles on Organic-Inorganic Hybrid Materials. *The Chemical Record*, *18*(7–8), 1222–1231. https://doi.org/10.1002/tcr.201800007

Takahashi, M., Suzuki, K., Tokudome, Y., Malfatti, L., & Innocenzi, P. (2014). Responsive microstructures on organic–inorganic hybrid films. *Journal of Sol-Gel Science and Technology*, *70*(2), 272–277. https://doi.org/10.1007/s10971-014-3301-0

Tan, W. K., Ito, T., Kawamura, G., Muto, H., Lockman, Z., & Matsuda, A. (2017). Controlled facile fabrication of plasmonic enhanced Au-decorated ZnO nanowire arrays dye-sensitized solar cells. *Materials Today Communications*, *13*, 354–358. https://doi.org/10.1016/j.mtcomm.2017.11.004

Tan, W. K., Muto, H., Ito, T., Kawamura, G., Lockman, Z., & Matsuda, A. (2020). Facile Fabrication of Plasmonic Enhanced Noble-Metal-Decorated ZnO Nanowire Arrays for Dye-Sensitized Solar Cells. *Journal of Nanoscience and Nanotechnology*, *20*(1), 359–366. https://doi.org/10.1166/jnn.2020.17223

Tan, W. K., Muto, H., Kawamura, G., Lockman, Z., & Matsuda, A. (2021). Nanomaterial Fabrication through the Modification of Sol–Gel Derived Coatings. *Nanomaterials*, *11*(1), 181. https://doi.org/10.3390/nano11010181

Tawa, S., Sato, Y., Orikasa, Y., Matsumoto, K., & Hagiwara, R. (2019). Lithium fluoride/iron difluoride composite prepared by a fluorolytic sol–gel method: Its electrochemical behavior and charge–discharge mechanism as a cathode material for lithium secondary batteries. *Journal of Power Sources*, *412*, 180–188. https://doi.org/10.1016/j.jpowsour.2018.11.046

Toe, M. Z., Pung, S. Y., Yaacob, K. A., Matsuda, A., Tan, W. K., & Han, S. S. (2020). Effect of TiO2 sol on the conversion efficiency of TiO2 based dye-sensitized solar cell. *Journal of Sol-Gel Science and Technology*, *95*(2), 439–446. https://doi.org/10.1007/s10971-020-05325-9

Torres Delgado, G., Zúñiga Romero, C. I., Mayén Hernández, S. A., Castanedo Pérez, R., & Zelaya Angel, O. (2009). Optical and structural properties of the sol–gel-

prepared ZnO thin films and their effect on the photocatalytic activity. *Solar Energy Materials and Solar Cells*, *93*(1), 55–59. https://doi.org/10.1016/j.solmat.2008.03.020

Valverde-Aguilar, G., & Manríquez Zepeda, J. L. (2015). Photoluminescence and photoconductivity studies on amorphous and crystalline ZnO thin films obtained by sol–gel method. *Applied Physics A*, *118*(4), 1305–1313. https://doi.org/10.1007/s00339-014-8836-y

Xu, L., Shi, L., & Li, X. (2009). Preparation of nanocone ZnO thin film and its aging effect of photoluminescence. *Applied Surface Science*, *255*(11), 5957–5960. https://doi.org/10.1016/j.apsusc.2009.01.044

Zou, G., Chen, W., Liu, R., & Xu, Z. (2007). Orientation enhancement of polycrystalline ZnO thin films through thermal oxidation of electrodeposited zinc metal. *Materials Letters*, *61*(21), 4305–4308. https://doi.org/10.1016/j.matlet.2007.01.092

[e-Saintika] Submission Acknowledgement

External Inbox ×

Muhammad Roil Bilad, Ph ... Jul 30, 2021, 10:38 PM
to me, Sukainil, Darminto

Hello,

Saiful Prayogi has submitted the manuscript, "Synthe
Characterization of ZnO Thin Layers using Sol-Gel S
to Jurnal Penelitian dan Pengkajian Ilmu Pendidikan:

If you have any questions, please contact me. Thank
this journal as a venue for your work.

Muhammad Roil Bilad, Ph.D

Pengkajian Ilmu Pendidikan: e-Saintika | Journal of F
Education Studies: e-Saintika

Sukainil Ahzan <sukainilahzan... Jul 31, 2021, 8:10 AM
to Ph.D, me, Darminto

Thanks a lot.

Submissions
Issues
Announcements

Settings
Journal
Website
Workflow
Distribution
Users & Roles

Statistics
Articles
Editorial Activity
Users
Reports

Tools

Workflow | **Publication**

Submission | Review | Copyediting | Production

Submission Files

Search

1753 sprayogi, 4 Artikel ZnO Spin Coating - Ahzan e-Saintika ING.docx	July 30, 2021	Article Text	

Download All Files

Pre-Review Discussions

Add discussion

Name	From	Last Reply	Replies	Closed
Your article	pejman 2021-07-31 03:30 PM	sprayogi 2021-07-31 03:44 PM	1	☐

Submissions

Issues

Announcements

Settings

Journal

Website

Workflow

Distribution

Users & Roles

Statistics

Articles

Editorial Activity

Users

Reports

Tools

Round 1

Round 1 Status

Submission accepted.

Reviewer's Attachments

Search

1776 , Initial Review.docx	July 31, 2021	

Revisions

Search Upload File

▸	1780 Article Text, 6 Revised.docx	August 5, 2021	Article Text
▸	1788 Article Text, 8 Revised_FN trackchnge(1).docx	August 17, 2021	Article Text

Review Discussions

Add discussion

Name	From	Last Reply	Replies	Closed

No Items

Synthesis and Characterization of ZnO Thin Layers using Sol-Gel Spin Coating Method

[1]Sukainil Ahzan, [2]Darminto, [1*]Saiful Prayogi

[1]Faculty of Applied Science and Engineering, Universitas Pendidikan Mandalika (Undikma), Jl. Pemuda No. 59A, Mataram 83126, Indonesia.
[2]Faculty of Mathematics and Science, Institut Teknologi Sepuluh Nopember (ITS), Jl. Raya ITS, Surabaya 60111, Indonesia.

Corresponding author email: saifulprayogi@ikipmataram.ac.id

Abstract: This study aimeds to synthesize a thin layer of ZnO material using the sol-gel spin coating method. This method ~~is~~ claimed to be low-cost with a simple fabrication process. A thin layer of ZnO was deposited on a glass substrate by the sol-gel spin coating method, then the quality of the ZnO layer was analyzed due to the influence of heating variables, rotation speed, and aging under ~~3~~ three days. The thin layer characterization included identification of the formed phase using X-Ray Diffractometer (XRD), the layered microstructure and elemental composition were observed using Scanning Electron Microscopy (SEM) coupled with EDS (Energy Dispersive Spectrometer). The ~~results of the study~~study results showed that a thin layer of ZnO was successfully deposited on a glass substrate by heat treatment at temperatures of 300°C and 500°C. XRD results show that the higher heating temperature has resulted in higher diffraction peak intensity. On the other hand, the higher coating rotation speed has ~~resulted in~~ a lower ~~the~~ intensity of diffraction peak. For the ZnO layer with aging variations of 0, 10, 24, 48, and 72 hours, the intensity was relatively stable. SEM results show that the surface morphology of the ZnO layer heated at 500°C has an average grain size of 300 nm. Based on the cross-sectional results of SEM shows that the higher the coating rotation speed has resulted the thinner of the ZnO layer, where the thickness of the resulting layer is on ~~the order~~ order> 5 μm.

***Keywords**: synthesis, characterization, ZnO thin film, sol-gel spin coating*

Introduction

~~In recent decades, as the demand for energy continues to increase, there has been tremendous interest in the development of renewable energy sources and environmentally friendly technological device systems, some of which include fuel cells, solar cells, supercapacitors, and efficient batteries.~~ In recent decades, as the demand for energy continues to increase, there has been tremendous interest in ~~the development of renewable energy sources and environmentally friendly technological device systems, some of which include fuel cells, solar cells, supercapacitors,~~developing renewable energy sources and environmentally friendly technological device systems, some of which include fuel-cells, solar-cells, supercapacitors, etc. and efficient batteries (Tan et al., 2021). In accordance with the interest in many fields of application, thin layers of several materials have been developed by the sol-gel method (Soo et al., 2013a, 2013b). Since being introduced by Groove in 1852, thin layer technology has undergone many developments in terms of manufacturing methods, materials used, and applications (Greene, 2017). In the thin layer processing technique, the material commonly used is metal (Jittiarporn et al., 2017; Mironyuk et al., 2020; Shi et al., 2020; Tan et al., 2020), organic, inorganic, and hybrid (Kawamura et al., 2010; Nisticò et al., 2017; Takahashi, 2018; Takahashi et al., 2014).

The advancement of thin films by the sol-gel method for various applications is highly dependent on the material used. In fuel-cell applications, PDDA films and microparticles of $PhSiO_{3/2}$ succeeded in increasing proton conductivity to achieve a stable proton supply (Daiko et al., 2008). Likewise, Pt/TiO_2 was developed as an electrocatalyst for fuel-cell electrolyte membrane applications (Nbelayim et al., 2020). The performance of a lightweight, high-capacity battery is

developed from the synthesis of Li/Ti double alkoxides in a $Li_4Ti_5O_{12}$ thin film (Mosa & Aparicio, 2020), and LiF/FeF_2 in the form of $Li0.5FeF_3$ (S. W. Kim et al., 2012; Tawa et al., 2019). Formation of superhydrophobic/superhydrophilic layers in film fabrication including surface design and film coating using Al_2O_3, ZrO_2, and TiO_2 materials (Tadanaga et al., 2004), these three materials were also developed in the technology of forming porous ceramics films from ZrO_2 (Soo et al., 2013a, 2013b), Al_2O_3 (Carstens & Enke, 2019), $SrTiO_3$ (Katagiri et al., 2012), some are also developed from SiO_2 material (Xie et al., 2021) and SiC (Ebrahimpour et al., 2014). Porous ceramics films are applied in adsorption technology and biomedical drug delivery (Katagiri et al., 2012; Shimogaki et al., 2016)~~,~~ and cosmetics (Chen et al., 2015). In addition, the development of thin films by the sol-gel method is used in the extraction technology of waste disposal, especially heavy metal adsorbents, such as electro-spined flexible Fe_3O_4 fibers (Shi et al., 2020)~~,~~ and yttria-stabilized ZrO2 membranes (Qin et al., 2020). The most extensively researched is the application of thin layers as solar-cells (~~dye~~ dye-sensitized solar cells/DSSC) (Abd-Ellah et al., 2016; Nbelayim et al., 2017, 2018, 2020; Tan et al., 2017; Toe et al., 2020), from zinc oxide material (ZnO) (Khan et al., 2017; Muchuweni et al., 2017; Prasada Rao et al., 2010).

Sol-gel coating techniques commonly used are spray coating, dip coating, roll coating, and spin coating (Tan et al., 2021). Several other methods are also used, such as molecular beam epitaxy (Wang et al., 2009), RF magnetron sputtering (S. Kim et al., 2006), pulsed laser deposition (Zhu et al., 2010), spray pyrolysis (Muchuweni et al., 2017; Prasada Rao et al., 2010), chemical vapor deposition (Singh et al., 2008), physical vapor deposition (George et al., 2010)~~, and t~~. The most frequently used is the sol-gel spin-coating method (Khan et al., 2017). The sol-gel spin coating method has several advantages compared to other methods, this is because the cost is low, the composition is homogeneous, does not use space with a high level of vacuum, the thickness of the layer can be controlled and the good microstructure (Cheng et al., 2003). The spin coating method has long been introduced by Brinker, which is the development of dip coating (Brinker et al., 1991). Sol-gel spin coting is a method for making layers of photoresist polymer materials deposited on the surface of silicon and other materials in the form of wafers (flat materials). After the solution (sol-gel) is dripped onto the wafer, the rotational speed is regulated by centrifugal force to produce a homogeneous thin layer. This sol-gel spin coating method combines simple physical and chemical methods. This method is very easy and effective to make thin films, by only setting the parameters of time, rotational speed, and viscosity of the solution.

From the several components of thin film-forming materials, zinc oxide (ZnO) is the most extensively studied~~,~~ because this material is one of the transparent semi-conductive oxides. (Zou et al., 2007), with a relatively high exciton binding energy (60 mEV) and a wide band gap around of 3.2 to 3.4 eV (Rwenyagila et al., 2014; Sivaramakrishnan & Alford, 2010; Valverde-Aguilar & Manríquez Zepeda, 2015). These advantages of optical and electrical properties allow ZnO to be applied as optical waveguides, optoelectronic devices (Çopuroğlu et al., 2009; Khan et al., 2017; Rwenyagila et al., 2014), piezoelectricity, conductive gas sensors, transparent conductive electrodes, photocatalysts and DSSC (Djurišić et al., 2010). One of the ~~interesting~~ exciting properties of ZnO to observe is the crystal formation process that occurs at temperatures under 400°C. This phenomenon depends on the type of deposition and the solvent used. Previous studies showed that the crystal structure of ZnO was formed using ethylene glycol and glycerol as a solvent at a heating temperature of 200°C (Torres Delgado et al., 2009). Heating at temperatures below 300°C is an early stage of heating, where the crystal structure has been formed but has not been oriented perfectly. Furthermore, with higher heating at 400°C and 500°C, the ZnO crystal structure

will be perfectly oriented (Raoufi & Raoufi, 2009). Another ~~interesting~~ attractive property of ZnO to observe is aging. Aging is the storage of sol-gel for a certain time before being used as a coating material. The aging process affects the physical, electrical, and optical properties of the ZnO thin film (Xu et al., 2009).

Literature review shows that the properties of ZnO thin films deposited by the sol-gel technique have not been studied adequately (Khan et al., 2017). In this study, we developed a thin layer of ZnO material by the sol-gel spin coating method ~~which is claimed to be~~, which is a cost-effective method and a simple fabrication process. The variables that are the focus of this study include heat treatment, rotation speed, rotation time, and aging. A thin layer of ZnO was deposited on a glass substrate by the sol-gel spin coating method, then the quality of the ZnO layer was analyzed due to the influence of heating variables, rotation speed, and aging under ~~3~~ three days.

Methods

A thin layer was deposited on a glass substrate with a size of 5 x 10 mm. The coating material is a sol-gel made from zinc acetate dehydrate $\{Zn(CH_3COO)_2.2H_2O\}$ powder with a molar ratio of MEA to ZnAc used is 1:1. The solvent used ethanol (C_2H_6O) and, as a stabilizer, used ethanolamine (MEA: C_2H_7NO), each with a purity of 99%. The solution was prepared by magnetic stirring at ±70°C for 30 minutes until the solution was homogeneously mixed.

When ZnAc is added to ethanol, a cloudy white solution appears. ZnAc is rather difficult to dissolve in ethanol~~,~~ ~~t~~. Therefore the dissolution process must be accompanied by heating. Heating is carried out on a hot~~-~~ plate with a temperature range of 80 to 100°C. The addition of MEA liquid little by little, makes the solution clear. After the heating process for 30 to 40 minutes, obtained a clear and transparent solution. The solution was then allowed to stand at room temperature to form a gel. The resulting solution in the form of a gel is divided into five parts and each is aged for 0, 10, 24, 48 and 72 hours.

The thermal behavior of ZnO gel was tested using Differential Thermal Analysis (DTA) and Thermogravimetric Analysis (TGA). This analysis aims to observe changes in energy and mass changes due to ~~changes in temperature~~temperature changes. The ~~results of the DTA/TGA analysis~~DTA/TGA analysis results can be used as a reference in determining the temperature at which the phase transformation occurs.

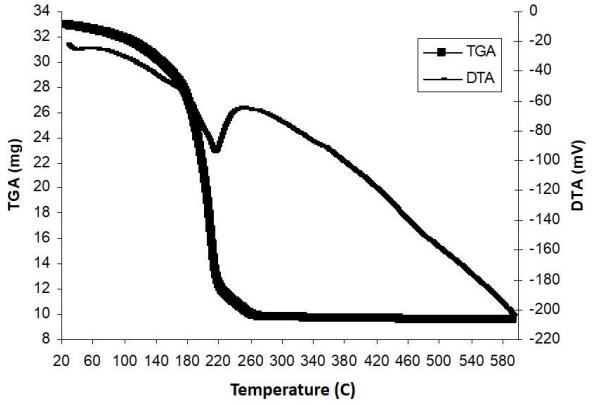

Figure 1. DTA-TGA test results of ZnO sol-gel.

Based on the results of the TGA (Fig. 1), it can be seen that the decrease in mass occurred about 90% of the initial mass, and after a temperature of 280°C, there was no further decrease in mass. Based on the DTA and TGA graphs, it is estimated that the change of ZnO + H_2O into ZnO crystals occurs on heating above 280°C, so that the ZnO layer pre-heating process can be carried out at a temperature of 300°C.

The deposition of a thin layer on a glass substrate with spin coating was also carried out at ~~variations of 1500, 2000, and 2500 rpm~~1500, 2000, and 2500 rpm variations. A thin layer of ZnO is heated using a furnace. The heating process is carried out in 3 stages~~, t~~. The first heating for 1 hour at a temperature of 100°C (calcination)~~,~~ aims to gradually remove the water content and residual solvent in the layer. The second heating was at 300°C, where the temperature was slowly increased from room temperature to 300°C for 5 hours, then held at that temperature for 6 minutes. This stage is ~~said to be a pre-heating stage which functions to remove solvents from ethanol, water, MEA, and facilitates the~~a pre-heating stage that functions to remove solvents from ethanol, water, MEA, and facilitates ZnO's conversion of ZnOH to ZnO. The next stage is post-heating or final heating at a temperature of 500°C. ~~Similar to~~Like the pre-heating process, the temperature rise is set slowly from room temperature to 500°C for 10 hours, then held at that temperature for 10 minutes. This post-heating function is to form ZnO particles with uniform crystal orientation~~,~~ and eliminate the pores.

The characterization of the coating results includes identification of the formed phase using X-~~Ray~~ ray Diffractometer (XRD), layer microstructure, and elemental composition observed by Scanning Electron Microscopy (SEM) coupled with EDS (Energy Dispersive Spectrometer).

Results and Discussion

3.1 Glass substrate characterization

The substrate used is glass preparations. Before use, the substrate is cleaned with a solution of detergent and ethanol. Each washing is carried out in an ultrasonic cleaner for 30 minutes, ~~which~~ that aime~~d~~s to thoroughly clean the dirt and oil content attached to the substrate. After that, the XRD and XRF tests were carried out.

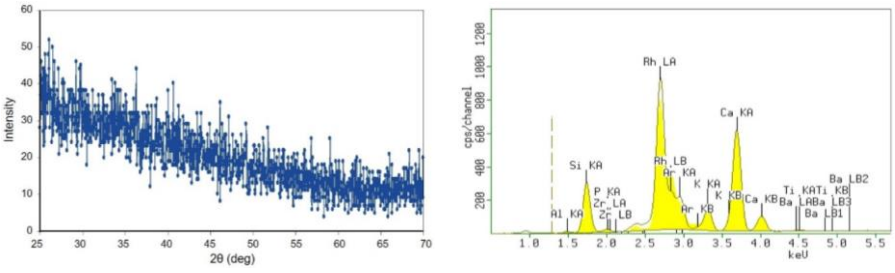

(a) (b)

Figure 2. Glass substrate characterization; a) XRD pattern; and b) XRF results.

The XRD results of the glass substrate are shown in Figure 2a. Based on the XRD data, it can be seen that there are no peaks formed. This indicates that the glass substrate has an amorphous structure. The XRF results of the glass substrate are shown in Figure 2b. The glass elements contain

silicon (Si), calcium Ca, and potassium (K), as well as several other elements (such as P, Ti, and Ba) with very small ~~intensity~~intensities. ~~Based on the XRD and XRF test results, it shows~~The XRD and XRF test results show that the glass substrate used is an amorphous material~~s~~.

3.2 Effect of heating on the ZnO crystal layer

The X-ray diffraction pattern of the ZnO layer deposited at 2000 rpm and aging for 24 hours on the variations in heating temperature is shown in Figure 3.

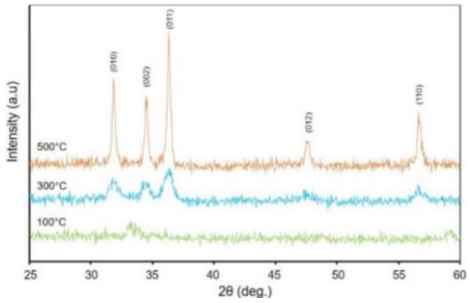

Figure 3. XRD pattern of ZnO layer with the variation of heating temperature

Based on Figure 3, it can be seen that the layer heated at a temperature of 100°C formed two peaks, namely at an angle of 33.15° and 59.30°. With the search match program, information was obtained that the peak with an angle of 33.15° is the zinc propianate ($C_6H_{10}O_4Zn$) phase, while the angle of 59.30° is the zinc salicylate dihydrete $\{(C_6H_{10}O_6Zn).2H_2O\}$ phase. This peak does not correspond to the peak of the ZnO crystal. This is caused the layer still contains a lot of water and solvents.

At a heating temperature of 300°C crystals have formed~~,~~ but are not yet perfectly oriented, ~~while at a temperature of 500°C~~at a 500(C), the ZnO crystals are perfectly oriented. This is consistent with the results of DTA-TGA (Fig. 1) that the formation of ZnO is above 280°C. With the help of the Rietica program, hexagonal ZnO has been formed with lattice parameters for a temperature of 300°C (a = 3,245 Å, c = 5,209 Å) and a temperature of 500°C (a = 3,249 Å, c = 5,205 Å). In the range of 2θ (from 25° to 60°), crystal plane peaks are formed, indicating that the layer obtained is polycrystalline.

Pre-heating and post-heating affect the ZnO layer in solvent evaporation and reaction material decomposition. At low pre-heating temperature (< 300°C), the diffraction peaks appeared (100), (002), and (101) with random preferential growth. This happens because at this temperature, the reagents have completely evaporated, and the thermal decomposition of the precursors has not yet occurred at this temperature~~, but~~. Still, they occur at post-heating temperatures above 500°C (Suwanboon et al., 2008). The increase in the intensity of the diffraction peak at higher temperatures~~,~~ due to the high temperature will produce greater energy to increase the movement of atoms, ~~resulting in an increase in~~increasing the quality and crystallization of the layer (Mandal et al., 2008).

3.3 Effect of spin coating speed on ZnO layer

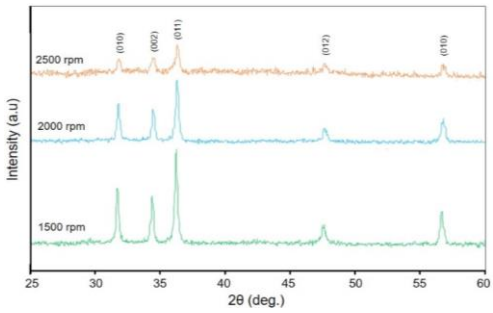

Figure 4. The XRD pattern of the ZnO layer was created with variations in rotational speed.

Figure 4 shows XRD results for ZnO layers made with variations in rotational speed of 1500, 2000, and 2500 rpm. The XRD peaks of the three samples show a change in intensity. The change that occurs is a decrease in intensity along with an increase in rotation speed. This happens because ZnO crystallization is easier to form in the coating process with a lower rotation (1500 rpm).

3.4 Effect of aging on ZnO crystal layer

The XRD pattern of the synthesized ZnO layer with variations in aging is presented in Figure 5. Before being used as a coating material, the gel material was stored for 0, 10, 24, 48, and 72 hours.

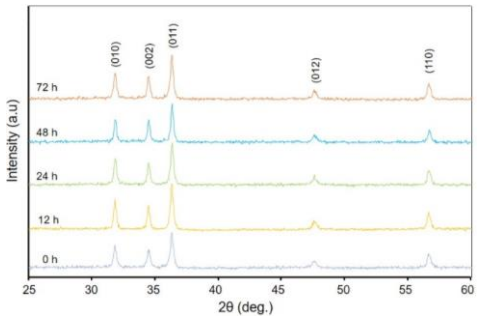

Figure 5. XRD pattern of deposited ZnO layer with an aging variation.

Based on Figure 5, there is no significant change in each layer, both in terms of intensity and width of the ZnO crystal peak. These results indicate that aging for less than ~~2~~ two days can form ZnO crystals. The results of another study reported that after aging for ~~7~~ seven days, the peak intensity (002) of ZnO increased compared to samples without aging and aging for ~~2~~ two days (Maldonado et al., 2010). After ~~3~~ three weeks of aging, ~~the peak intensity (002) of ZnO~~ZnO's peak intensity

(002) increased compared to the sample without aging (Fathollahi & Amini, 2001). This may occur because aging can cause further condensation of active groups and ~~aggregation of Z~~ZnO aggregation in solution and cause significant growth at peak intensity (002) of ZnO (Fathollahi & Amini, 2001).

The morphology and crystal structure of the ZnO layer made by the sol-gel process is influenced by the solvent, pre-heating and post-heating temperatures, sol concentration, substrate, and coating process (Habibi & Khaledi Sardashti, 2008). The ~~nucleation thermodynamics and crystal growth of the ZnO layer~~ZnO layer's nucleation thermodynamics and crystal growth showed a transformation from an amorphous to crystalline state. The growth of crystals with the dominant c-axis orientation depends on the surface energy of the layer and the glass substrate and the interfacial energy between them. In crystal growth, ~~fast growing fields generally depend on the loss of slow-~~growing fields depend on the loss of ~~slow-~~growing fields~~fields~~, with lower surface energies.

3.5 Surface morphology of ZnO thin layer

SEM photos of the ZnO layer surface heated at 100, 300, and 500°C, respectively, are presented in Figure 6.

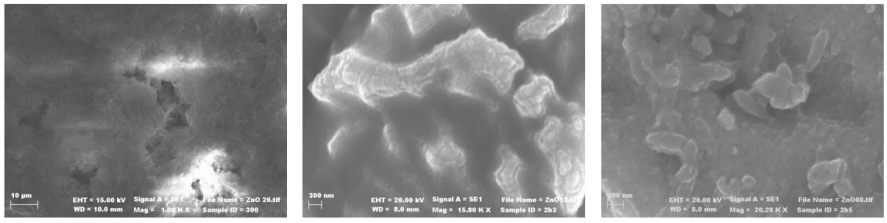

(a) (b) (c)

Figure 6. SEM photos of the ZnO layer surface heated at: (a) 100°C, (b) 300°C, and (c) 500°C.

At a temperature of 100°C (Fig. 6a), the layer is still coarse and porous, with a pore size of approximately 6 µm – 8 µm. This is because ~~at this temperature the layer still contains water molecules and solvents that have not completely evaporated~~the layer still contains water molecules and solvents that have not completely evaporated at this temperature~~. W~~, when the layer is heated at 300°C (pre-heating), the remaining organic matter can evaporate completely, and ZnO grains begin to grow (Fig. 6b), but the distance between the particles is still ~~quite~~ relatively large. When the ZnO layer is heated at 500°C (Fig. 6c), the atoms in the existing grains receive sufficient driving force energy to diffuse to form new, larger grains. As a result of this inter-grain diffusion, necking will be formed ~~which results~~, resulting in the shrinking of the boundary between grains and porosity (Fig. 6c). The average grain size at this temperature is about 300 nm.

In addition to heat treatment, the morphology and thickness of the ZnO layer are also affected by the spin coating speed. Figure 7 shows the surface morphology of the coated layer at 1500, 2000, and 2500 rpm.

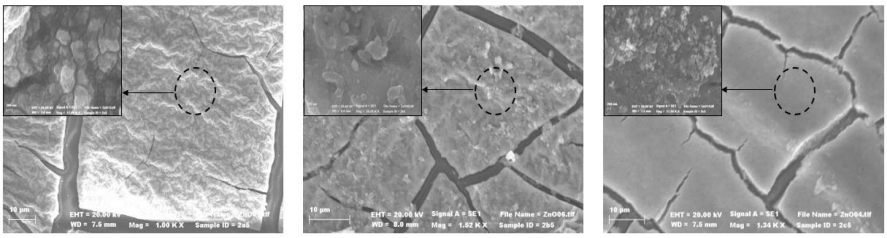

(a) (b) (c)

Figure 7. SEM photos of the ZnO layer surface coated with variations in rotation speed: (a) 1500 rpm, (b) 2000 rpm, and (c) 2500 rpm.

Based on Figure 7, it can be seen that the higher the rotation speed, the smoother the coating obtained, with the average grain size getting smaller. The ZnO layer coated at 1500 and 2000 rpm had almost the same average grain size, ~~which was~~ 300 nm, while the ZnO layer coated at 2500 rpm had an average grain size of 100 nm. Previous studies reported that the higher the rotational speed used to make the ZnO layer, the smaller of grain size produced (Ilican et al., 2008). The cross-sectional analysis of the coated ZnO layer with variations in rotational speed is presented in Figure 8.

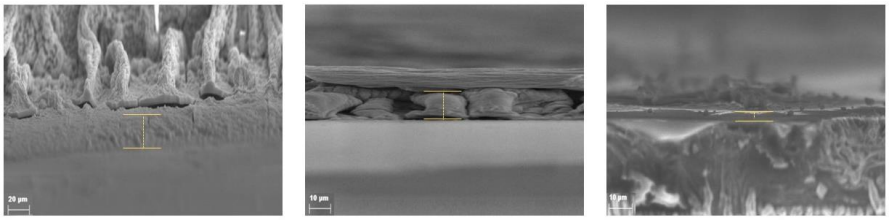

(a) (b) (c)

Figure 8. Cross-section of the coated ZnO layer with variations in rotational speed: (a) 1500 rpm, (b) 2000 rpm, and (c) 2500 rpm.

The results in Figure 8a show that the thickness of the ZnO layer coated with 1500 rpm rotation is about 30 μm, while the layer coated with 2000 rpm rotation is about 20 μm (Fig. 8b), 2500 rpm at about 5 μm (Fig. 8c). So it can be stated that the thickness of the ZnO layer gets thinner as the rotation speed increases. In ~~the process of~~ forming a ~~layer~~ coating on the substrate, it takes a large enough centrifugal speed to distribute the gel over the entire surface~~,~~ and remove the excess gel to the outside of the substrate. If the rotational speed is increased, the previously attached gel will be thrown out of the substrate, and the layer will thin out, or it can also disappear. This is because the binding force between the substrate and the gel is not strong enough to withstand the centrifugal force, which is too high. So, the faster the coating rotation, the more gel will leave the substrate so that the resulting layer is thinner.

From the results in Figure 7, although the layer looks smooth, most of the areas in the layer have many micron-sized cracks. Cracks that are microns in size and can only be seen with an optical

microscope or SEM are called microcracks. These cracks are caused by the uneven heating rate on the surface of the coating and the thermal coefficient between the substrate and the coating is not the same. Cracks also occur in the area between the layer and the substrate (Fig. 7). Based on the cross-sectional photo of the ZnO layer (Fig. 8), it can be seen that the layer is not completely attached to the substrate. This results in the quality of the bond between the coating and the substrate being less strong, so that when the coating is exposed to scratches or friction from the outside it will cause the coating to peel off easily. Cracks can also be seen from the EDX results (see Fig. 9). Based on the results of the EDX, there is an elemental content of Ca (0.98% wt) in the crack section, namely the elements contained in the substrate (from XRF results). Although the Ca content is small, this still indicates that the cracks are ~~very deep~~intense until they penetrate the ZnO layer. Based on Figure 9, it is estimated that the thickness of the ZnO layer formed on heating at 500°C is about 5 μm to 20 μm. The size of this layer is thick, so this ZnO layer cannot be classified as a thin layer (< 1 μm).

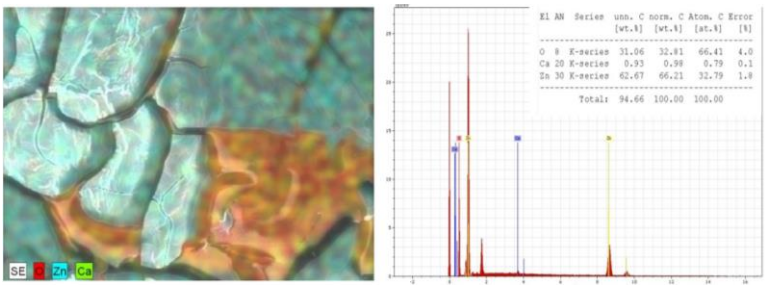

(a) (b)

Figure 9. EDX results of ZnO layer on a glass substrate: (a) surface topography, and (b) elemental content.

Microcracks may occur on the ~~surface of the ceramic coating~~ceramic coating surface with the cracks spreading along the grain boundaries (Sakka, 2018). This happens because the layer and the substrate have a ~~very lar~~huge difference in the coefficient of thermal expansion. The spread of microcracks along the grain boundaries is formed before the crystallization process. These microcracks can be prevented by equalizing the coefficient of thermal expansion (α) between the coating and the substrate. For example BaTiO3 (α =140 x 10^{-7} K^{-1}), the layer has microcracks when deposited on a SiO2 glass substrate (α = 5 x 10^{-7} K^{-1}), but BaTiO3 has no microcracks on a single crystal substrate of MgO (α = 135 x 10^{-7} K^{-1}) (Sakka, 2018). Microcracks can occur during the heating process at low temperatures (100°C - 400°C). In another study (Kozuka & Hirano, 2000) reported that in the production of the titania layer, the crystal structure appears at a temperature of 500°C, while cracks appear at temperatures below it. This means that the crack occurs before the crystallization process.

Microcracks can also occur due to variations in the thickness of the gel layer. In the titania layer made with variations in thickness, the thicker layer is obtained, which tends to crack at low temperatures (Kozuka & Hirano, 2000). This happens because the thickness affects the occurrence of intrinsic stress during the heating process. ~~Crack~~ The crack formation also depends on the heating rate. Cracks appear at higher temperatures when the coating is heated at a low heating

rate. A~~t a~~ low heating, the rate will produce a smaller porosity. This indicates that the low heating rate allows sufficient time for the coating to solidify during heating resulting in high tensile stresses in the substrate plane.

Conclusion

The ZnO layer was successfully deposited on a glass substrate by heat treatment at ~~temperatures of~~ 300°C and 500°C. At a heating temperature of 100°C, the ZnO structure has not yet been formed, and when the heating temperature is 300°C, crystals have started to form but have not been oriented perfectly. ZnO crystals are perfectly oriented at 500°C. XRD results show that the higher heating temperature has resulted in higher diffraction peak intensity. The higher the coating rotation speed, the lower the intensity. For the ZnO layer with aging variations of 0, 10, 24, 48, and 72 hours, the intensity was relatively stable. SEM results show that the surface morphology of the ZnO layer heated at 500°C has an average grain size of 300 nm. ~~Based on the cross sectional results of SEM shows~~The cross-sectional results of SEM show that the higher the rotation speed, the thinner the resulting ZnO layer, where the thickness of the resulting layer is on the order of > 5 μm.

Recommendation

here

Commented [AM1]: Please present the recommendation based on your research finding

Acknowledgment

here

Commented [AM2]: Fill this section too

References

Abd-Ellah, M., Moghimi, N., Zhang, L., Thomas, Joseph. P., McGillivray, D., Srivastava, S., & Leung, K. T. (2016). Plasmonic gold nanoparticles for ZnO-nanotube photoanodes in dye-sensitized solar cell application. *Nanoscale*, *8*(3), 1658–1664. https://doi.org/10.1039/C5NR08029K

Brinker, C. J., Frye, G. C., Hurd, A. J., & Ashley, C. S. (1991). Fundamentals of sol-gel dip coating. *Thin Solid Films*, *201*(1), 97–108. https://doi.org/10.1016/0040-6090(91)90158-T

Carstens, S., & Enke, D. (2019). Investigation of the formation process of highly porous α-Al2O3 via citric acid-assisted sol-gel synthesis. *Journal of the European Ceramic Society*, *39*(7), 2493–2502. https://doi.org/10.1016/j.jeurceramsoc.2019.01.043

Chen, Q., Li, W., Goudouri, O.-M., Ding, Y., Cabanas-Polo, S., & Boccaccini, A. R. (2015). Electrophoretic deposition of antibiotic loaded PHBV microsphere-alginate composite coating with controlled delivery potential. *Colloids and Surfaces B: Biointerfaces*, *130*, 199–206. https://doi.org/10.1016/j.colsurfb.2015.04.009

Cheng, Z., Zhang, J., & Kronmüller, H. (2003). Magnetically soft phase in magnetization reversal processes of nanocomposite Sm 2 Fe 15 Ga 2 C x / α − Fe permanent magnetic materials. *Physical Review B*, *68*(14), 144417. https://doi.org/10.1103/PhysRevB.68.144417

Çopuroğlu, M., Koh, L. H. K., O'Brien, S., & Crean, G. M. (2009). Comparative characterisation of zinc oxide thin films prepared from zinc acetate with or without water of hydration via the sol–gel method. *Journal of Sol-Gel Science and Technology*, *52*(3), 432–438. https://doi.org/10.1007/s10971-009-2016-0

Daiko, Y., Sakamoto, H., Katagiri, K., Muto, H., Sakai, M., & Matsuda, A. (2008). Deposition of Ultrathin Nafion Layers on Sol–Gel-Derived Phenylsilsesquioxane Particles via Layer-by-Layer Assembly. *Journal of The Electrochemical Society*, *155*(5), B479. https://doi.org/10.1149/1.2885101

Djurišić, A. B., Ng, A. M. C., & Chen, X. Y. (2010). ZnO nanostructures for optoelectronics: Material properties and device applications. *Progress in Quantum Electronics*, *34*(4), 191–259. https://doi.org/10.1016/j.pquantelec.2010.04.001

Ebrahimpour, O., Dubois, C., & Chaouki, J. (2014). Fabrication of mullite-bonded porous SiC ceramics via a sol–gel assisted in situ reaction bonding. *Journal of the European Ceramic Society*, *34*(2), 237–247. https://doi.org/10.1016/j.jeurceramsoc.2013.08.028

Fathollahi, V., & Amini, M. M. (2001). Sol–gel preparation of highly oriented gallium-doped zinc oxide thin films. *Materials Letters*, *50*(4), 235–239. https://doi.org/10.1016/S0167-577X(01)00231-2

George, A., Kumari, P., Soin, N., Roy, S. S., & McLaughlin, J. A. (2010). Microstructure and field emission characteristics of ZnO nanoneedles grown by physical vapor deposition. *Materials Chemistry and Physics*, *123*(2–3), 634–638. https://doi.org/10.1016/j.matchemphys.2010.05.029

Greene, J. E. (2017). Review Article: Tracing the recorded history of thin-film sputter deposition: From the 1800s to 2017. *Journal of Vacuum Science & Technology A: Vacuum, Surfaces, and Films*, *35*(5), 05C204. https://doi.org/10.1116/1.4998940

Habibi, M. H., & Khaledi Sardashti, M. (2008). Structure and morphology of nanostructured zinc oxide thin films Prepared by dip-vs. Spin-coating methods. *Journal of the Iranian Chemical Society*, *5*(4), 603–609. https://doi.org/10.1007/BF03246140

Ilican, S., Caglar, Y., & Caglar, M. (2008). Preparation and Characterization Of ZnO Thin Films Deposited By Sol-Gel Spin Coating Method. *Journal of Optoelectronics and Advanced Materials*, *10*(10), 2578–2583.

Jittiarporn, P., Badilescu, S., Al Sawafta, M. N., Sikong, L., & Truong, V.-V. (2017). Electrochromic properties of sol–gel prepared hybrid transition metal oxides – A short review. *Journal of Science: Advanced Materials and Devices*, *2*(3), 286–300. https://doi.org/10.1016/j.jsamd.2017.08.005

Katagiri, K., Kamiya, J., Koumoto, K., & Inumaru, K. (2012). Preparation of hollow titania and strontium titanate spheres using sol–gel derived silica gel particles as templates. *Journal of Sol-Gel Science and Technology*, *63*(3), 366–372. https://doi.org/10.1007/s10971-012-2795-6

Kawamura, G., Sato, S., Muto, H., Sakai, M., Lim, P. B., Watanabe, K., Inoue, M., & Matsuda, A. (2010). AgBr nanocrystal-dispersed silsesquioxane–titania hybrid films for holographic materials. *Materials Letters*, *64*(23), 2648–2651. https://doi.org/10.1016/j.matlet.2010.08.068

Khan, M. I., Bhatti, K. A., Qindeel, R., Alonizan, N., & Althobaiti, H. S. (2017). Characterizations of multilayer ZnO thin films deposited by sol-gel spin coating technique. *Results in Physics*, *7*, 651–655. https://doi.org/10.1016/j.rinp.2016.12.029

Kim, S., Jeong, M.-C., Oh, B.-Y., Lee, W., & Myoung, J.-M. (2006). Fabrication of Zn/ZnO nanocables through thermal oxidation of Zn nanowires grown by RF magnetron sputtering. *Journal of Crystal Growth*, *290*(2), 485–489. https://doi.org/10.1016/j.jcrysgro.2006.01.043

Kim, S. W., Nam, K. W., Seo, D. H., Hong, J., Kim, K., Gwon, H., & Kang, K. (2012). Energy storage in composites of a redox couple host and a lithium ion host. *Nano Today*, *7*(3), 168–173. https://doi.org/10.1016/j.nantod.2012.04.004

Kozuka, H., & Hirano, M. (2000). Radiative Striations and Surface Roughness of Alkoxide-Derived Spin Coating Films. *Journal of Sol-Gel Science and Technology*, *19*(1/3), 501–504. https://doi.org/10.1023/A:1008772102546

Maldonado, A., Tirado-Guerra, S., Cázares, J. M., & Olvera, M. de la L. (2010). Physical and sensing properties of ZnO:F:Al thin films deposited by sol–gel. *Thin Solid Films*, *518*(7), 1815–1820. https://doi.org/10.1016/j.tsf.2009.09.039

Mandal, S., Goswami, M. L. N., Das, K., Dhar, A., & Ray, S. K. (2008). Temperature dependent photoluminescence characteristics of nanocrystalline ZnO films grown by sol–gel technique. *Thin Solid Films*, *516*(23), 8702–8706. https://doi.org/10.1016/j.tsf.2008.05.016

Mironyuk, I., Mykytyn, I., Vasylyeva, H., & Savka, K. (2020). Sodium-modified mesoporous TiO2: Sol-gel synthesis, characterization and adsorption activity toward heavy metal cations. *Journal of Molecular Liquids*, *316*, 113840. https://doi.org/10.1016/j.molliq.2020.113840

Mosa, J., & Aparicio, M. (2020). Sol-Gel Synthesis of Nanocrystalline Mesoporous Li4Ti5O12 Thin-Films as Anodes for Li-Ion Microbatteries. *Nanomaterials*, *10*(7), 1369. https://doi.org/10.3390/nano10071369

Muchuweni, E., Sathiaraj, T. S., & Nyakotyo, H. (2017). Synthesis and characterization of zinc oxide thin films for optoelectronic applications. *Heliyon*, *3*(4), e00285. https://doi.org/10.1016/j.heliyon.2017.e00285

Nbelayim, P., Ashida, Y., Maegawa, K., Kawamura, G., Muto, H., & Matsuda, A. (2020). Preparation and Characterization of Stable and Active Pt@TiO $_2$ Core–Shell Nanoparticles as Electrocatalyst for Application in PEMFCs. *ACS Applied Energy Materials*, *3*(4), 3269–3281. https://doi.org/10.1021/acsaem.9b02169

Nbelayim, P., Kawamura, G., Abdel-Galeil, M. M., Tan, W. K., Wei, X., Muto, H., & Matsuda, A. (2018). Effects of multi-sized and -shaped Ag@TiO_2 nanoparticles on the performance of plasmonic dye-sensitized solar cells. *Journal of the Ceramic Society of Japan*, *126*(3), 139–151. https://doi.org/10.2109/jcersj2.17203

Nbelayim, P., Kawamura, G., Kian Tan, W., Muto, H., & Matsuda, A. (2017). Systematic characterization of the effect of Ag@TiO2 nanoparticles on the performance of plasmonic dye-sensitized solar cells. *Scientific Reports*, *7*(1), 15690. https://doi.org/10.1038/s41598-017-15541-z

Nisticò, R., Scalarone, D., & Magnacca, G. (2017). Sol-gel chemistry, templating and spin-coating deposition: A combined approach to control in a simple way the porosity of inorganic thin films/coatings. *Microporous and Mesoporous Materials*, *248*, 18–29. https://doi.org/10.1016/j.micromeso.2017.04.017

Prasada Rao, T., Santhosh Kumar, M. C., Safarulla, A., Ganesan, V., Barman, S. R., & Sanjeeviraja, C. (2010). Physical properties of ZnO thin films deposited at various substrate temperatures using spray pyrolysis. *Physica B: Condensed Matter*, *405*(9), 2226–2231. https://doi.org/10.1016/j.physb.2010.02.016

Qin, H., Guo, W., Huang, X., Gao, P., & Xiao, H. (2020). Preparation of yttria-stabilized ZrO2 nanofiltration membrane by reverse micelles-mediated sol-gel process and its application in pesticide wastewater treatment. *Journal of the European Ceramic Society*, *40*(1), 145–154. https://doi.org/10.1016/j.jeurceramsoc.2019.09.023

Raoufi, D., & Raoufi, T. (2009). The effect of heat treatment on the physical properties of sol–gel derived ZnO thin films. *Applied Surface Science*, *255*(11), 5812–5817. https://doi.org/10.1016/j.apsusc.2009.01.010

Rwenyagila, E. R., Agyei-Tuffour, B., Zebaze Kana, M. G., Akin-Ojo, O., & Soboyejo, W. O. (2014). Optical properties of ZnO/Al/ZnO multilayer films for large area transparent electrodes. *Journal of Materials Research*, *29*(24), 2912–2920. https://doi.org/10.1557/jmr.2014.298

Sakka, S. (2018). Sol-Gel Formation of Bulk Glasses. In L. Klein, M. Aparicio, & A. Jitianu (Eds.), *Handbook of Sol-Gel Science and Technology* (pp. 233–256). Springer International Publishing. https://doi.org/10.1007/978-3-319-32101-1_6

Shi, S., Xu, C., Wang, X., Xie, Y., Wang, Y., Dong, Q., Zhu, L., Zhang, G., & Xu, D. (2020). Electrospinning fabrication of flexible Fe3O4 fibers by sol-gel method with high saturation magnetization for heavy metal adsorption. *Materials & Design*, *186*, 108298. https://doi.org/10.1016/j.matdes.2019.108298

Shimogaki, T., Tokoro, H., Tabuchi, M., Koike, N., Yamashina, Y., & Takahashi, M. (2016). Large-scale preparation of morphology-controlled microporous silica particles via gradual injection of reactants with different surfactants. *Journal of Sol-Gel Science and Technology*, *79*(3), 440–446. https://doi.org/10.1007/s10971-015-3942-7

Singh, P., Kumar, A., Deepak, & Kaur, D. (2008). ZnO nanocrystalline powder synthesized by ultrasonic mist-chemical vapour deposition. *Optical Materials*, *30*(8), 1316–1322. https://doi.org/10.1016/j.optmat.2007.06.012

Sivaramakrishnan, K., & Alford, T. L. (2010). Conduction and transmission analysis in gold nanolayers embedded in zinc oxide for flexible electronics. *Applied Physics Letters*, *96*(20), 201109. https://doi.org/10.1063/1.3435467

Soo, M. T., Kawamura, G., Muto, H., Matsuda, A., Lockman, Z., & Cheong, K. Y. (2013a). Design of hierarchically meso–macroporous tetragonal ZrO2 thin films with tunable thickness by spin-coating via sol–gel template route. *Microporous and Mesoporous Materials*, *167*, 198–206. https://doi.org/10.1016/j.micromeso.2012.09.010

Soo, M. T., Kawamura, G., Muto, H., Matsuda, A., Lockman, Z., & Cheong, K. Y. (2013b). Fabrication of well-crystallized mesoporous ZrO2 thin films via Pluronic P123 templated sol–gel route. *Ceramics International*, *39*, S437–S440. https://doi.org/10.1016/j.ceramint.2012.10.109

Suwanboon, S., Tanattha, R., & Tanakorn, R. (2008). Fabrication and properties of nanocrystalline zinc oxide thin film prepared by sol-gel method. *Songklanakarin Journal of Science and Technology*, *30*(1), 65–69.

Tadanaga, K., Fujii, T., Matsuda, A., Minami, T., & Tatsumisago, M. (2004). Micropatterning of Sol-Gel Derived Thin Films Using Hydrophobic-Hydrophilic Patterned Surface. *Journal of Sol-Gel Science and Technology*, *31*(1–3), 299–302. https://doi.org/10.1023/B:JSST.0000048007.43110.fa

Takahashi, M. (2018). Responsive and Adaptive Micro Wrinkles on Organic-Inorganic Hybrid Materials. *The Chemical Record*, *18*(7–8), 1222–1231. https://doi.org/10.1002/tcr.201800007

Takahashi, M., Suzuki, K., Tokudome, Y., Malfatti, L., & Innocenzi, P. (2014). Responsive microstructures on organic–inorganic hybrid films. *Journal of Sol-Gel Science and Technology*, *70*(2), 272–277. https://doi.org/10.1007/s10971-014-3301-0

Tan, W. K., Ito, T., Kawamura, G., Muto, H., Lockman, Z., & Matsuda, A. (2017). Controlled facile fabrication of plasmonic enhanced Au-decorated ZnO nanowire arrays dye-sensitized solar cells. *Materials Today Communications*, *13*, 354–358. https://doi.org/10.1016/j.mtcomm.2017.11.004

Tan, W. K., Muto, H., Ito, T., Kawamura, G., Lockman, Z., & Matsuda, A. (2020). Facile Fabrication of Plasmonic Enhanced Noble-Metal-Decorated ZnO Nanowire Arrays for Dye-Sensitized Solar Cells. *Journal of Nanoscience and Nanotechnology*, *20*(1), 359–366. https://doi.org/10.1166/jnn.2020.17223

Tan, W. K., Muto, H., Kawamura, G., Lockman, Z., & Matsuda, A. (2021). Nanomaterial Fabrication through the Modification of Sol–Gel Derived Coatings. *Nanomaterials*, *11*(1), 181. https://doi.org/10.3390/nano11010181

Tawa, S., Sato, Y., Orikasa, Y., Matsumoto, K., & Hagiwara, R. (2019). Lithium fluoride/iron difluoride composite prepared by a fluorolytic sol–gel method: Its electrochemical behavior and charge–discharge mechanism as a cathode material for lithium secondary batteries. *Journal of Power Sources*, *412*, 180–188. https://doi.org/10.1016/j.jpowsour.2018.11.046

Toe, M. Z., Pung, S. Y., Yaacob, K. A., Matsuda, A., Tan, W. K., & Han, S. S. (2020). Effect of TiO2 sol on the conversion efficiency of TiO2 based dye-sensitized solar cell. *Journal of Sol-Gel Science and Technology*, *95*(2), 439–446. https://doi.org/10.1007/s10971-020-05325-9

Torres Delgado, G., Zúñiga Romero, C. I., Mayén Hernández, S. A., Castanedo Pérez, R., & Zelaya Angel, O. (2009). Optical and structural properties of the sol–gel-prepared ZnO thin films and their effect on the photocatalytic activity. *Solar Energy Materials and Solar Cells*, *93*(1), 55–59. https://doi.org/10.1016/j.solmat.2008.03.020

Valverde-Aguilar, G., & Manríquez Zepeda, J. L. (2015). Photoluminescence and photoconductivity studies on amorphous and crystalline ZnO thin films obtained by sol–gel method. *Applied Physics A*, *118*(4), 1305–1313. https://doi.org/10.1007/s00339-014-8836-y

Wang, C., Chen, Z., Hu, H., & Zhang, D. (2009). Effect of the oxygen pressure on the microstructure and optical properties of ZnO films prepared by laser molecular beam epitaxy. *Physica B: Condensed Matter*, *404*(21), 4075–4082. https://doi.org/10.1016/j.physb.2009.07.165

Xie, Y.-T., Chen, J.-R., Chen, Y.-T., Jiang, B.-C., Sie, Z.-H., Hsu, H.-Y., Chen, T.-L., Chiang, Y.-Y., & Hsueh, H.-Y. (2021). Sol–gel-derived hierarchically wrinkled mesoporous ceramics for enhancement of cell alignment. *Chemical Engineering Journal*, *405*, 126572. https://doi.org/10.1016/j.cej.2020.126572

Xu, L., Shi, L., & Li, X. (2009). Preparation of nanocone ZnO thin film and its aging effect of photoluminescence. *Applied Surface Science*, *255*(11), 5957–5960. https://doi.org/10.1016/j.apsusc.2009.01.044

Zhu, B. L., Zhao, X. Z., Su, F. H., Li, G. H., Wu, X. G., Wu, J., & Wu, R. (2010). Low temperature annealing effects on the structure and optical properties of ZnO films grown by pulsed laser deposition. *Vacuum*, *84*(11), 1280–1286. https://doi.org/10.1016/j.vacuum.2010.01.059

Zou, G., Chen, W., Liu, R., & Xu, Z. (2007). Orientation enhancement of polycrystalline ZnO thin films through thermal oxidation of electrodeposited zinc metal. *Materials Letters*, *61*(21), 4305–4308. https://doi.org/10.1016/j.matlet.2007.01.092

Synthesis and Characterization of ZnO Thin Layers using Sol-Gel Spin Coating Method

[1]Sukainil Ahzan, [2]Darminto, [3]Ferry Anggoro Ardy Nugroho, [1*]Saiful Prayogi

[1]Faculty of Applied Science and Engineering, Universitas Pendidikan Mandalika (Undikma), Jl. Pemuda No. 59A, Mataram 83126, Indonesia.
[2]Faculty of Mathematics and Science, Institut Teknologi Sepuluh Nopember (ITS), Jl. Raya ITS, Surabaya 60111, Indonesia.
[2]Departmet of Physics and Astronomy, Vrije Universiteit Amsterdam, De Boelelaan 1081, 1081 HV Amsterdam, The Netherlands.

Corresponding author email: saifulprayogi@ikipmataram.ac.id

Abstract: The potential of thin layer in many applications has led to research on the development of many new materials and their fabrication methods. This study aimed to synthesize a thin layer of ZnO using the facile and low-cost sol-gel spin coating method. The ZnO thin layer is deposited on a glass substrate and analyzed to observe the influence of the deposition variables such as heating and rotation speed, and its aging. The characterization methods include the identification of the formed phase using X-Ray Diffractometer (XRD), and the microstructure and elemental composition using Scanning Electron Microscopy (SEM) coupled with EDS (Energy Dispersive Spectrometer). The study shows that a thin layer of ZnO is successfully deposited on a glass substrate by heat treatment at temperatures of 300 °C and 500 °C. Furthermore, XRD reveals that higher heating temperatures result in higher diffraction peak intensity. At a heating temperature of 300 °C crystals are formed but are not yet perfectly oriented. At 500 °C, the ZnO crystals are perfectly oriented. On the other hand, higher spin coating rotation speed gives rise to lower intensity of diffraction peak. The ZnO crystallization is easier to form in the coating process with a lower rotation (1500 rpm). Interestingly, the thin layer is stable over time where there is no significant change in each sample, both in terms of intensity and width of the ZnO crystal peak. The results indicate that gel precursor aged less than two days can form ZnO crystals. Finally, SEM results show that the surface morphology of the ZnO layer heated at 500 °C has an average grain size of 300 nm. Based on the cross-sectional results of SEM shows that the higher the coating rotation speed has resulted the thinner of the ZnO layer, where the thickness of the resulting layer is on order >5 μm.

***Keywords**: synthesis, characterization, ZnO thin ~~film~~layer, sol-gel spin coating*

Formatted: Font: 10 pt
Formatted: Font: 10 pt
Formatted: Font: 10 pt
Formatted: Font: 10 pt
Formatted: Font: 10 pt
Formatted: Font: 10 pt
Formatted: Font: 10 pt

Introduction

In recent decades, as the demand for energy continues to increase, there has been tremendous interest in developing renewable energy sources and environmentally friendly technological device systems (Matsuda & Kawamura, 2016), some of which include fuel-cells, solar-cells, supercapacitors, etc. and efficient batteries (Tan et al., 2021). In accordance with the interest in many fields of application, thin layers of several materials have been developed by the sol-gel method (Soo et al., 2013a, 2013b). Since being introduced by Groove in 1852, thin layer technology has undergone many developments in terms of manufacturing methods, materials used, and applications (Greene, 2017). In the thin layer processing technique, the material commonly used is metal (Jittiarporn et al., 2017; Mironyuk et al., 2020; Shi et al., 2020; Tan et al., 2020), organic, inorganic, and hybrid (organic-inorganic) (Kawamura et al., 2010; Nisticò et al., 2017; Takahashi, 2018; Takahashi et al., 2014).

The advancement of thin films by the sol-gel method for various applications is highly dependent on the material used. In fuel-cell applications, for example, PDDA films and microparticles of $PhSiO_{3/2}$ succeeded in increasing proton conductivity to achieve a stable proton supply (Daiko et al., 2008). Likewise, Pt/TiO_2 was demonstrated as an electrocatalyst for fuel-cell electrolyte

membrane applications (Nbelayim et al., 2020). The performance of a lightweight, high-capacity battery is developed from the synthesis of Li/Ti double alkoxides in a $Li_4Ti_5O_{12}$ thin film (Mosa & Aparicio, 2020), and LiF/FeF_2 in the form of $Li0.5FeF_3$ (Kim et al., 2012; Tawa et al., 2019). Formation of superhydrophobic/superhydrophilic layers in film fabrication including surface design and film coating using Al_2O_3, ZrO_2, and TiO_2 materials (Tadanaga et al., 2004)~~, these three materials were also developed in the technology of forming porous ceramics films from ZrO_2 (Soo et al., 2013a, 2013b), Al_2O_3 (Carstens & Enke, 2019), $SrTiO_3$ (Katagiri et al., 2012), some are also developed from SiO_2 material (Xie et al., 2021) and SiC (Ebrahimpour et al., 2014). Porous ceramics films are applied in adsorption technology and biomedical drug delivery (Katagiri et al., 2012; Shimogaki et al., 2016) and cosmetics (Chen et al., 2015)~~. In addition, the development of thin films by the sol-gel method is used in the extraction technology of waste disposal, especially heavy metal adsorbents , such as electro-spined flexible Fe_3O_4 fibers (Shi et al., 2020) and yttria-stabilized ZrO_2 membranes (Qin et al., 2020). The most extensively researched is the application of thin layers as solar-cells (dye-sensitized solar cells/DSSC) (Abd-Ellah et al., 2016; Nbelayim et al., 2017, 2018, 2020; Tan et al., 2017; Toe et al., 2020), from zinc oxide material (ZnO) (Khan et al., 2017; Muchuweni et al., 2017; Prasada Rao et al., 2010).

Formatted: Subscript

Sol-gel coating techniques commonly used include spray coating, dip coating, roll coating, and spin coating (Tan et al., 2021). Among these, spin-coating method is the most frequently used (Khan et al., 2017). This method combines simple physical and chemical methods and has several advantages compared to other methods, for instance being cost-efficient with relatively simple setup, and excellent control over the thickness (through parameters of time, rotational speed, and viscosity of the solution) and the homogeneity of the layer (Cheng et al., 2003).

Among thin film-forming materials, zinc oxide (ZnO) is the most extensively studied because it is one of the transparent semi-conductive oxides (Zou et al., 2007) with a relatively high exciton binding energy (60 mEV) and a wide band gap around of 3.2 to 3.4 eV (Rwenyagila et al., 2014; Sivaramakrishnan & Alford, 2010; Valverde-Aguilar & Manríquez Zepeda, 2015). These advantages of optical and electrical properties allow ZnO to be applied as optical waveguides, optoelectronic devices (Çopuroğlu et al., 2009; Khan et al., 2017; Rwenyagila et al., 2014), piezoelectricity, conductive gas sensors, transparent conductive electrodes, photocatalysts and DSSC (Djurišić et al., 2010). One of the exciting properties of ZnO is its crystal formation process that occurs at temperatures under 400 °C. This phenomenon depends on the type of deposition and the solvent used. Previous studies showed that crystalline ZnO was formed using ethylene glycol and glycerol as a solvent at a heating temperature of 200 °C (Torres Delgado et al., 2009). Heating at temperatures below 300°C is an early stage of heating, where the crystal structure has been formed but has not been oriented perfectly. Furthermore, with higher heating at 400 °C and 500 °C, the ZnO crystal structure will be perfectly oriented (Raoufi & Raoufi, 2009). Another attractive property of ZnO to observe is aging. Aging is the storage of sol-gel for a certain time before being used as a coating material. The aging process affects the physical, electrical, and optical properties of the ZnO thin film (Xu et al., 2009).

Literature surveys reveal that reports on the properties of ZnO thin films deposited by the sol-gel technique is lacking (Khan et al., 2017). Here, we develop a thin layer of ZnO material by the sol-gel spin coating method and assess its crystallization properties and morphology~~xxxx properties~~. The variables that are the focus of this study include heat treatment, rotation speed~~, rotation time~~, and aging. ~~We find that xxxx (Kasih highlight highligt dari finding di paper ini)~~

Formatted: Font: (Default) Calisto MT, 11 pt, Font color: Auto, English (United States), Pattern: Clear

Formatted: Not Highlight

Formatted: Font: (Default) Calisto MT, 11 pt, Font color: Auto, English (United States), Pattern: Clear

Methods

A thin layer was deposited on a glass substrate of 5 x 10 mm^2 using a sol-gel method using zinc acetate dehydrate {$Zn(CH_3COO)_2.2H_2O$} powder (M: 219.49 g/mol, 99% Merck, Germany) with a molar ratio of 1:1 MEA:ZnAc. Ethanol (C_2H_6O) (99% technical, Merck) was used as solvent and ethanolamine (MEA: C_2H_7NO) as stabilizer, each with a purity of 99%. The solution was prepared by magnetic stirring at ±70 °C for 30 minutes. ZnAc was rather difficult to dissolve in ethanol. Therefore the dissolution process must be accompanied by heating, which was carried out on a hot plate with a temperature range of 80 to 100 °C. This was followed by the addition of MEA. After the heating process for 30 to 40 minutes, the solution was then allowed to stand at room temperature to form a gel. The gel was the divided into five parts and each was aged for 0, 10, 24, 48 and 72 hours. The gel have been aged in air with a room temperature of ±25°C and with 70±5% humidity.

The thermal behavior of ZnO gel was tested using Differential Thermal Analysis (DTA) and Thermogravimetric Analysis (TGA). This analysis aimed to observe changes in energy and mass as function of temperature. The DTA/TGA analysis results are used as a reference in determining the temperature at which the phase transformation occurs.

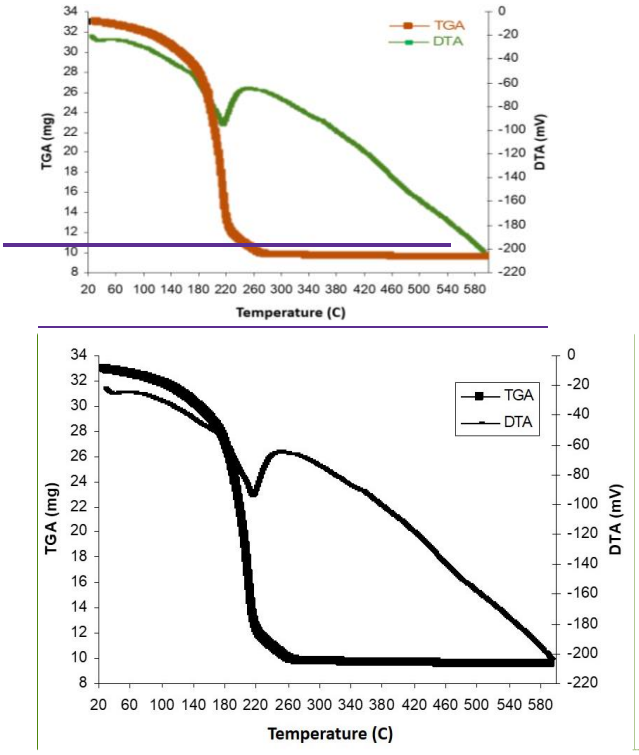

Figure 1. DTA-TGA test results of ZnO thin film deposited by spin coat sol-gel.

Based on the results of the TGA (Fig. 1), it can be seen that there is 90% decrease in massup to a temperature of 280 °C, after which there is no further decrease in mass. This decrease in mass is

Formatted: Normal, Line spacing: single, Don't adjust space between Latin and Asian text, Don't adjust space between Asian text and numbers

Formatted: Font: Calisto MT, 11 pt

Formatted: Font: Palatino Linotype

Formatted: Left

Commented [FN1]: Simbolnya tidak bisa dibedakan mana yang mana, bisa diganti warna saja

followed by energy release or endothermic (DTA Graph in Fig. 1). Based on the DTA and TGA graphs, it is estimated that the change of ZnO + H_2O into ZnO crystals occurs on heating above 280 °C, so that the ZnO layer pre-heating process can be carried out at a temperature of 300 °C.

The deposition of the thin layer on a glass substrate with spin coating was also carried out at 1500, 2000, and 2500 rpm variations. A thin layer of ZnO was heated using a furnace. The heating process was carried out in 3 stages. The first heating for 1 hour at a temperature of 100 °C (calcination) aimed to gradually remove the water content and residual solvent in the layer. The second heating at 300 °C, where the temperature was slowly increased from room temperature to 300 °C for 5 hours, was held for 6 minutes. This stage was a pre-heating stage that functioned to remove solvents from ethanol, water, MEA, and facilitated ZnOH conversion to ZnO. The next stage was post-heating or final heating at a temperature of 500 °C. Like the pre-heating process, the temperature rise was set slowly from room temperature to 500 °C in 10 hours, then held for 10 minutes. This post-heating functioned to form ZnO particles with uniform crystal orientation and eliminate the pores.

The characterization of the coating results included identification of the formed phase using X-ray Diffractometer (XRD) with the help of a search match and refinement program using Rietica software with the comparison is standard data (CPI ZnO 1011259), layer microstructure, and elemental composition observed by Scanning Electron Microscopy (SEM) coupled with EDS (Energy Dispersive Spectrometer).

Results and Discussion

~~***3.1 Glass substrate characterization***~~

~~The substrate used is glass preparations. Before use, the substrate is cleaned with a solution of detergent and ethanol. Each washing is carried out in an ultrasonic cleaner for 30 minutes, that aimed to thoroughly clean the dirt and oil content attached to the substrate. After that, the XRD and XRF tests were carried out.~~

Commented [FN2]: Bagian ini ga penting, bisa dihapus. Yg pentingcuma cleaning procedurnya aja bisa ditaruh di methods.

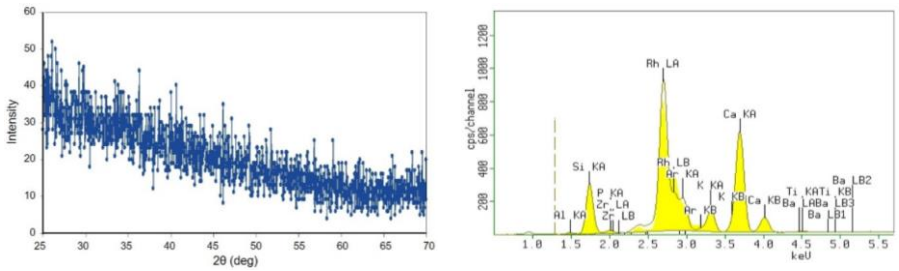

~~(a)~~ ~~(b)~~

~~**Figure 2**. Glass substrate characterization; a) XRD pattern; and b) XRF results.~~

~~The XRD results of the glass substrate are shown in Figure 2a. Based on the XRD data, it can be seen that there are no peaks formed. This indicates that the glass substrate has an amorphous structure. The XRF results of the glass substrate are shown in Figure 2b. The glass elements contain silicon (Si), calcium Ca, and potassium (K), as well as several other elements (such as P, Ti, and Ba) with very small intensities. The XRD and XRF test results show that the glass substrate used is an amorphous material.~~

3.~~2~~ 1 Effect of heating on the ZnO crystal layer

The X-ray diffraction pattern of the ZnO layer deposited at 2000 rpm at various heating temperature and aged for 24 hours is shown in Figure 2~~3~~.

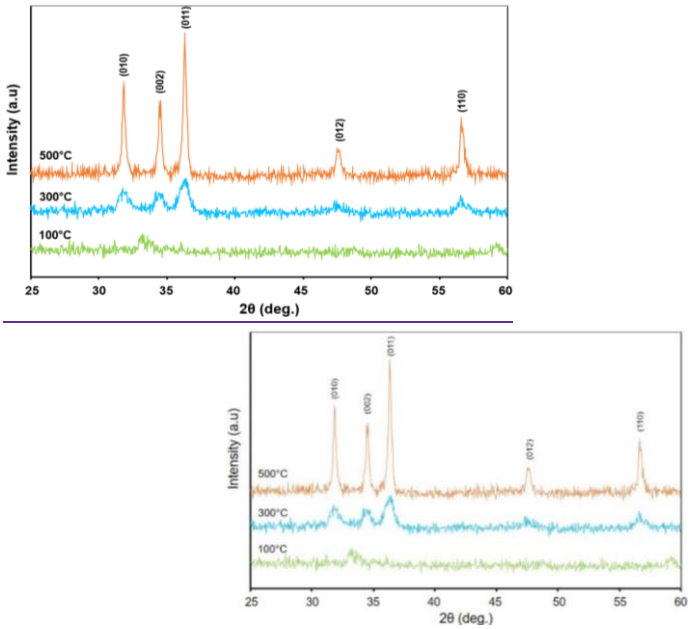

Figure ~~3~~2. XRD pattern of ZnO layer with the variation of heating temperature

Based on Figure ~~3~~2, it can be seen that the layer heated at a temperature of 100 °C forms two peaks at an angle of 33.15° and 59.30°. These peaks correspond to zinc propianate ($C_6H_{10}O_4Zn$) phase and zinc salicylate dihydrete $\{(C_6H_{10}O_6Zn).2H_2O\}$ phase, respectively. These peaks clearly originate from the solvents on the layer.

At a heating temperature of 300 °C crystals are formed but are not yet perfectly oriented. At 500 °C~~(C)~~, the ZnO crystals are perfectly oriented. This is consistent with the results of DTA-TGA (cf. Fig. 1) in that the formation of ZnO occurs above 280 °C. With the help of the Rietica program, hexagonal ZnO has been formed with lattice parameters for a temperature of 300 °C (a = 3,245 Å, c = 5,209 Å) and a temperature of 500°C (a = 3,249 Å, c = 5,205 Å). In the range of 2θ of 25° to 60°), crystal plane peaks are formed, indicating that the layer obtained is polycrystalline.

Pre- and post-heating affect the ZnO layer in the form of solvent evaporation and reaction material decomposition. At low pre-heating temperature (< 300 °C), the (100), (002), and (101) diffraction peaks appeared with random preferential growth. This happens because at this temperature, the reagents have completely evaporated, and the thermal decomposition of the precursors has not yet occurred. Still, they occur at post-heating temperatures above 500 °C (Suwanboon et al., 2008). The increase in the intensity of the diffraction peak at higher temperatures is due to greater energy

Formatted: Left

available to increase the movement of atoms, which increases the quality and crystallization of the layer (Mandal et al., 2008).

3.~~2~~ Effect of spin coating speed on ZnO layer

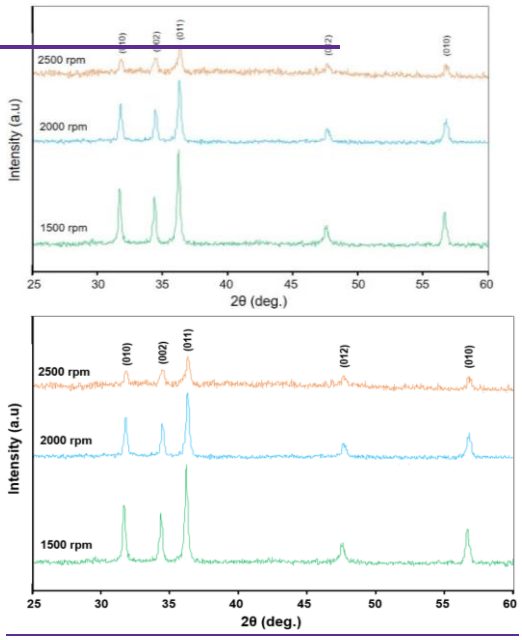

Figure ~~4~~3. The XRD pattern of the ZnO layer with variations in spin coat rotational speed.

Figure ~~4~~ 3 shows XRD results for ZnO layers made with variations in rotational speed of 1500, 2000, and 2500 rpm. The XRD peaks of the three samples show a decrease in intensity as rotation speed increases. This happens because ZnO crystallization is easier to form in the coating process with a lower rotation (1500 rpm).

3.~~4~~ 3 Effect of aging on ZnO crystal layer

The XRD pattern of the synthesized ZnO layer with variations in aging of the precursor gel is presented in Figure ~~5~~4.

Formatted: Left

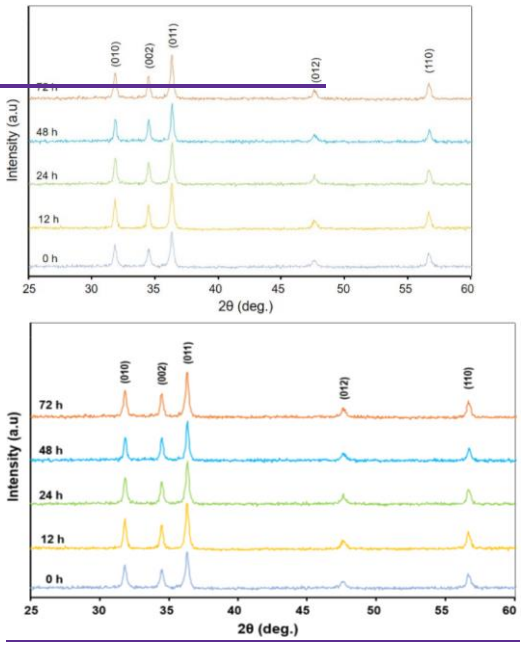

Figure ~~5~~4. XRD pattern of deposited ZnO layer with an aging variation.

Based on Figure ~~5~~4, there is no significant change in each sample, both in terms of intensity and width of the ZnO crystal peak. These results indicate that gel precursor aged less than two days can form ZnO crystals. The results of another study reported that after aging for seven days, the peak intensity (002) of ZnO increased compared to samples aged for up to two days (Maldonado et al., 2010). This may occur because aging can cause further condensation of active groups and ZnO aggregation in solution and cause significant growth at peak intensity (002) of ZnO (Fathollahi & Amini, 2001).

~~The morphology and crystal structure of the ZnO layer made by the sol gel process is influenced by the solvent, pre-heating and post-heating temperatures, sol concentration, substrate, and coating process (Habibi & Khaledi Sardashti, 2008). The ZnO layer's nucleation thermodynamics and crystal growth showed a transformation from an amorphous to crystalline state. The growth of crystals with the dominant c-axis orientation depends on the surface energy of the layer and the glass substrate and the interfacial energy between them. In crystal growth, growing fields depend on the loss ofslow growing fields, with lower surface energies.~~

3.~~5~~4 Surface morphology of ZnO thin layer

SEM photos of the ZnO layer surface heated at 100, 300, and 500 °C, respectively, are presented in Figure ~~6~~5.

Formatted: Left

Commented [FN3]: Info ini tidak relevan ada disini.

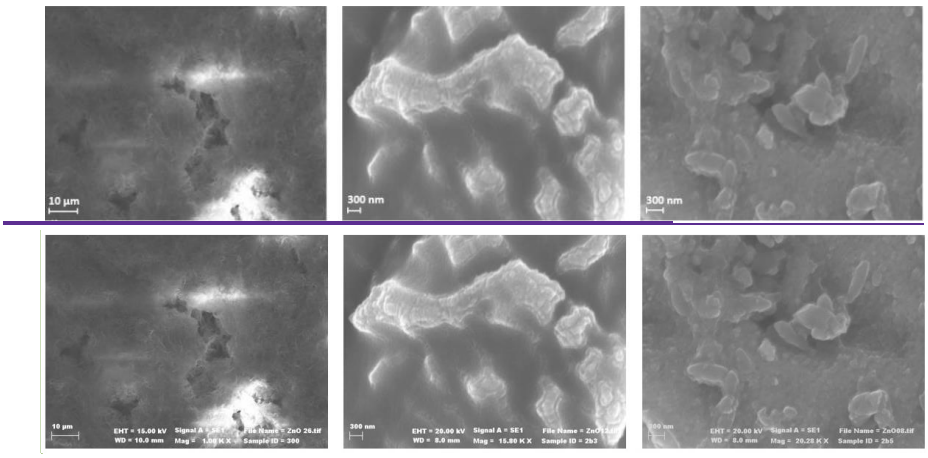

(a) (b) (c)

Figure ~~6~~5. SEM photos of the ZnO layer surface heated at: (a) 100°C, (b) 300°C, and (c) 500°C.

At a temperature of 100°C (Fig. ~~6a~~5a), the layer is still coarse and porous, with a pore size of approximately 6 µm – 8 µm. This is because the layer still contains water molecules and solvents that have not completely evaporated at this temperature. When the layer is heated at 300 °C (pre-heating), the remaining organic matter can evaporate completely, and ZnO grains begin to grow (Fig. ~~6b~~5b), but the distance between the particles is still relatively large. When the ZnO layer is heated at 500 °C (Fig. ~~6c~~5c), the atoms in the existing grains receive sufficient driving force energy to diffuse to form new, larger grains. As a result of this inter-grain diffusion, necking will be formed, resulting in the shrinking of the boundary between grains and porosity (Fig. ~~6c~~5c). The average grain size at this temperature is about 300 nm.

The morphology and crystal structure of the ZnO layer made by the sol-gel process is influenced by the solvent, pre-heating and post-heating temperatures, sol concentration, substrate, and coating process (Habibi & Khaledi Sardashti, 2008). The ZnO layer's nucleation thermodynamics and crystal growth showed a transformation from an amorphous to crystalline state. The growth of crystals with the dominant c-axis orientation depends on the surface energy of the layer and the glass substrate and the interfacial energy between them. In crystal growth, -growing fields depend on the loss of slow-growing fields, with lower surface energies.

In addition to heat treatment, the morphology and thickness of the ZnO layer are also affected by the spin coating speed. Figure ~~7~~6 shows the surface morphology of the coated layer at 1500, 2000, and 2500 rpm.

Formatted: Centered

Formatted Table

Commented [FN4]: Scale bar tidak terbaca, selain dari itu teks lain bisa dihilangkan.

Formatted: Indent: First line: 0 cm

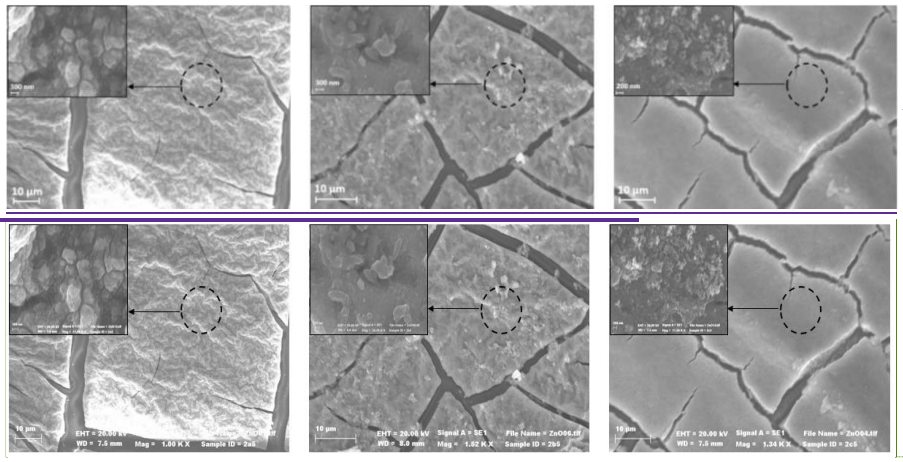

(a) (b) (c)

Figure ~~7~~6. SEM photos of the ZnO layer surface coated with variations in rotation speed: (a) 1500 rpm, (b) 2000 rpm, and (c) 2500 rpm.

Based on Figure ~~7~~6, it can be seen that the higher the rotation speed, the smoother the coating obtained, with smaller average grain size. The ZnO layer coated at 1500 and 2000 rpm has similar average grain size of 300 nm, while the ZnO layer coated at 2500 rpm has an average grain size of 100 nm. The results are consistent with previous studies that reported that the higher the rotational speed used to make the ZnO layer, the smaller of grain size produced (Ilican et al., 2008). The cross-sectional analysis of the coated ZnO layer with variations in rotational speed is presented in Figure ~~8~~7.

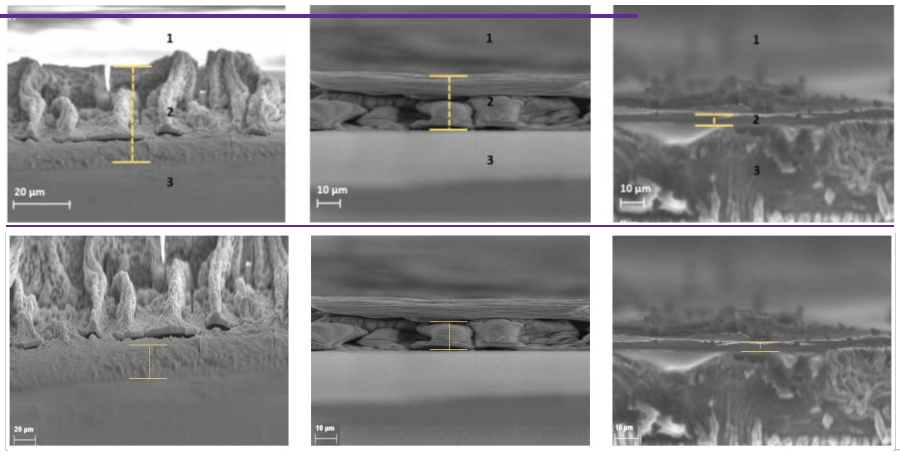

(a) (b) (c)

Figure ~~8~~7. Cross-section of the coated ZnO layer with variations in rotational speed: (a) 1500 rpm, (b) 2000 rpm, and (c) 2500 rpm. (1 = air, 2 = ZnO layer thickness, 3 = substrate)

Formatted Table

Commented [FN5]: Scale bar tidak terbaca (terlebih lagi bwt inset), selain dari itu teks lain bisa dihilangkan.

Formatted Table

Commented [FN6]: Legenda garis kuningnya tidak ada penjelasan itu apa. Scale bar juga tidak terbaca

The results show that the thickness of the ZnO layer coated with 1500 rpm rotation is about 30 μm (Fig. ~~8a~~7a), while the layer coated with 2000 rpm rotation is about 20 μm (Fig. ~~8b~~7b), 2500 rpm at about 5 μm (Fig. ~~8c~~7c). Therefore it can be stated that the thickness of the ZnO layer gets thinner as the rotation speed increases. In forming a coating on the substrate, it takes a large enough centrifugal speed to distribute the gel over the entire surface and remove the excess gel to the outside of the substrate. If the rotational speed is increased, the previously attached gel will be thrown out of the substrate, and the layer will thin out, or it can also disappear. This is because the binding force between the substrate and the gel is not strong enough to withstand the centrifugal force, which is too high. So, the faster the coating rotation, the more gel will leave the substrate so that the resulting layer is thinner.

From the results in Figure ~~7~~6, although the layer looks smooth, most of the areas in the layer have many micron-sized cracks. These cracks are caused by the uneven heating rate on the surface of the coating layer and the different thermal coefficient between the substrate and the coating layer. Cracks also occur in the area between the layer and the substrate (Fig. ~~7~~6). Based on the cross-sectional photo of the ZnO layer (Fig. 7~~8~~), it can be seen that the layer is not completely attached to the substrate. This condition makes the coating to peel off easily when exposed to scratches or friction from the outside. Cracks can also be seen from the EDX results (see Fig. ~~9~~8). From the Figure we also see existence of Ca (0.98% wt) in the cracks, that originates from the substrate (from ~~XRF results). Although the Ca content is small, this still indicat~~es that the cracks are intense they penetrate the ZnO layer. Based on the Figure ~~9~~8, it is estimated that the thickness of the ZnO layer formed with heating at 500 °C is about 5 μm to 20 μm.

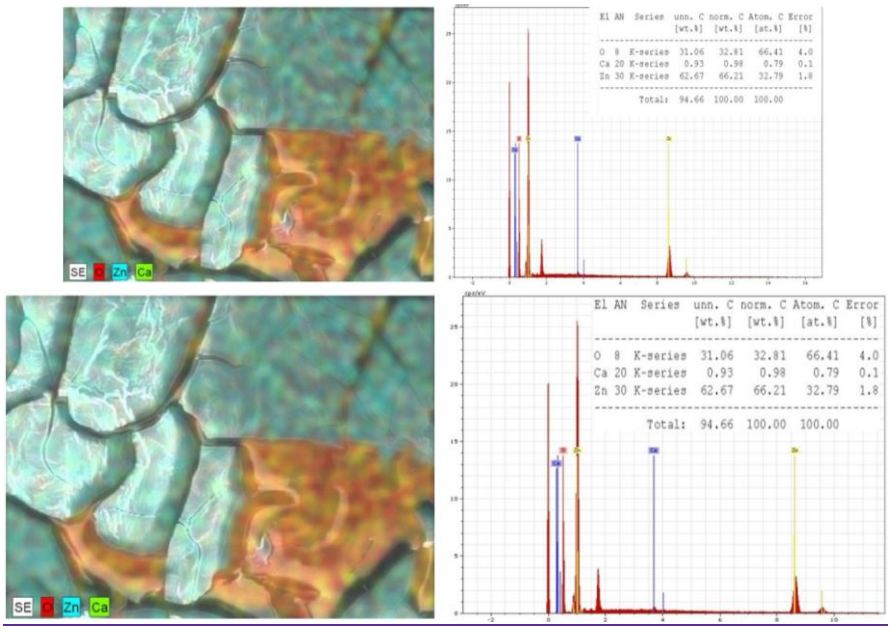

(a) (b)

Formatted Table

Figure ~~9~~8. EDX results of ZnO layer on a glass substrate: (a) surface topography, and (b) elemental content.

Microcracks may occur on the ceramic coating surface with the cracks spreading along the grain boundaries (Sakka, 2018). This phenomena happens because the layer and the substrate have a huge difference in the coefficient of thermal expansion. The spread of microcracks along the grain boundaries is formed before the crystallization process. These microcracks can be prevented by equalizing the coefficient of thermal expansion (α) between the coating and the substrate. For example BaTiO3 (α =140 x 10^{-7} K^{-1}), the layer has microcracks when deposited on a SiO2 glass substrate (α = 5 x 10^{-7} K^{-1}), but BaTiO3 has no microcracks on a single crystal substrate of MgO (α = 135 x 10^{-7} K^{-1}) (Sakka, 2018). Microcracks can occur during the heating process at low temperatures (100°C - 400°C). In another study (Kozuka & Hirano, 2000) reported that in the production of the titania layer, the crystal structure appears at a temperature of 500°C, while cracks appear at temperatures below it. This means that the crack occurs before the crystallization process.

Microcracks can also occur due to variations in the thickness of the gel layer. In the titania layer made with variations in thickness, the thicker layer is obtained, which tends to crack at low temperatures (Kozuka & Hirano, 2000). This happens because the thickness affects the occurrence of intrinsic stress during the heating process. The crack formation also depends on the heating rate. Cracks appear at higher temperatures when the coating is heated at a low heating rate. Alow heating, the rate will produce a smaller porosity. This indicates that the low heating rate allows sufficient time for the coating to solidify during heating resulting in high tensile stresses in the substrate plane.

Conclusion

The ZnO layer was successfully deposited on a glass substrate by heat treatment at 300 °C and 500 °C. At a heating temperature of 100°C, the ZnO structure has not yet been formed, and when the heating temperature is 300 °C, crystals have started to form but have not been oriented perfectly. ZnO crystals are perfectly oriented at 500 °C. XRD results show that the higher heating temperature has resulted in higher diffraction peak intensity. At a heating temperature of 300 °C crystals are formed but are not yet perfectly oriented. At 500 °C, the ZnO crystals are perfectly oriented. On the other hand, higher spin coating rotation speed gives rise to lower intensity of diffraction peak. The ZnO crystallization is easier to form in the coating process with a lower rotation (1500 rpm). Interestingly, the thin layer is stable over time where there is no significant change in each sample, both in terms of intensity and width of the ZnO crystal peak~~The higher the coating rotation speed, the lower the intensity. For the ZnO layer with aging variations of 0, 10, 24, 48, and 72 hours, the intensity was relatively stable~~. The results indicate that gel precursor aged less than two days can form ZnO crystals. SEM results show that the surface morphology of the ZnO layer heated at 500 °C has an average grain size of 300 nm. The cross-sectional results of SEM show that the higher the rotation speed, the thinner the resulting ZnO layer, where the thickness of the resulting layer is on ~~the~~ order ~~of~~ > 5 μm.

Formatted: Font: 11 pt

Formatted: Font: 11 pt

Formatted: Font: 11 pt

Formatted: Font: 11 pt

Formatted: Font: 11 pt

Commented [FN7]: Komen yg sama

Formatted: Font: 11 pt

Recommendation

The XRD results of the ZnO layer deposited on the glass substrate were all polycrystalline in structure. Efforts to make ZnO layer single crystal ~~with plane orientation (002)~~ must be continued, by proper selection of substrate and higher post-heating. In addition, the SEM results show that

the surface morphology of the ZnO layer is not homogeneous, there are many cracks and the size is still thick. For this reason, it is necessary to carry out more in-depth experiments in terms of the use of appropriate concentrations, speeds, and rotation times, as well as the selection of a substrate that has a heat capacity and plane orientation in accordance with the ZnO layer, for example alumina ceramic material.

Acknowledgment

here

Commented [AM8]: Fill this section too

References

Abd-Ellah, M., Moghimi, N., Zhang, L., Thomas, Joseph. P., McGillivray, D., Srivastava, S., & Leung, K. T. (2016). Plasmonic gold nanoparticles for ZnO-nanotube photoanodes in dye-sensitized solar cell application. *Nanoscale*, *8*(3), 1658–1664. https://doi.org/10.1039/C5NR08029K

Cheng, Z., Zhang, J., & Kronmüller, H. (2003). Magnetically soft phase in magnetization reversal processes of nanocomposite Sm 2 Fe 15 Ga 2 C x / α − Fe permanent magnetic materials. *Physical Review B*, *68*(14), 144417. https://doi.org/10.1103/PhysRevB.68.144417

Çopuroğlu, M., Koh, L. H. K., O'Brien, S., & Crean, G. M. (2009). Comparative characterisation of zinc oxide thin films prepared from zinc acetate with or without water of hydration via the sol–gel method. *Journal of Sol-Gel Science and Technology*, *52*(3), 432–438. https://doi.org/10.1007/s10971-009-2016-0

Daiko, Y., Sakamoto, H., Katagiri, K., Muto, H., Sakai, M., & Matsuda, A. (2008). Deposition of Ultrathin Nafion Layers on Sol–Gel-Derived Phenylsilsesquioxane Particles via Layer-by-Layer Assembly. *Journal of The Electrochemical Society*, *155*(5), B479. https://doi.org/10.1149/1.2885101

Djurišić, A. B., Ng, A. M. C., & Chen, X. Y. (2010). ZnO nanostructures for optoelectronics: Material properties and device applications. *Progress in Quantum Electronics*, *34*(4), 191–259. https://doi.org/10.1016/j.pquantelec.2010.04.001

Fathollahi, V., & Amini, M. M. (2001). Sol–gel preparation of highly oriented gallium-doped zinc oxide thin films. *Materials Letters*, *50*(4), 235–239. https://doi.org/10.1016/S0167-577X(01)00231-2

Greene, J. E. (2017). Review Article: Tracing the recorded history of thin-film sputter deposition: From the 1800s to 2017. *Journal of Vacuum Science & Technology A: Vacuum, Surfaces, and Films*, *35*(5), 05C204. https://doi.org/10.1116/1.4998940

Habibi, M. H., & Khaledi Sardashti, M. (2008). Structure and morphology of nanostructured zinc oxide thin films Prepared by dip-vs. Spin-coating methods. *Journal of the Iranian Chemical Society*, *5*(4), 603–609. https://doi.org/10.1007/BF03246140

Ilican, S., Caglar, Y., & Caglar, M. (2008). Preparation and Characterization Of ZnO Thin Films Deposited By Sol-Gel Spin Coating Method. *Journal of Optoelectronics and Advanced Materials*, *10*(10), 2578–2583.

Jittiarporn, P., Badilescu, S., Al Sawafta, M. N., Sikong, L., & Truong, V.-V. (2017). Electrochromic properties of sol–gel prepared hybrid transition metal oxides – A short review. *Journal of Science: Advanced Materials and Devices*, *2*(3), 286–300. https://doi.org/10.1016/j.jsamd.2017.08.005

Kawamura, G., Sato, S., Muto, H., Sakai, M., Lim, P. B., Watanabe, K., Inoue, M., & Matsuda, A. (2010). AgBr nanocrystal-dispersed silsesquioxane–titania hybrid films for holographic materials. *Materials Letters*, *64*(23), 2648–2651. https://doi.org/10.1016/j.matlet.2010.08.068

Khan, M. I., Bhatti, K. A., Qindeel, R., Alonizan, N., & Althobaiti, H. S. (2017). Characterizations of multilayer ZnO thin films deposited by sol-gel spin coating technique. *Results in Physics*, *7*, 651–655. https://doi.org/10.1016/j.rinp.2016.12.029

Formatted: Font: 11 pt

Formatted: Justified, Line spacing: Multiple 1,15 li

Kim, S. W., Nam, K. W., Seo, D. H., Hong, J., Kim, K., Gwon, H., & Kang, K. (2012). Energy storage in composites of a redox couple host and a lithium ion host. *Nano Today*, *7*(3), 168–173. https://doi.org/10.1016/j.nantod.2012.04.004

Kozuka, H., & Hirano, M. (2000). Radiative Striations and Surface Roughness of Alkoxide-Derived Spin Coating Films. *Journal of Sol-Gel Science and Technology*, *19*(1/3), 501–504. https://doi.org/10.1023/A:1008772102546

Maldonado, A., Tirado-Guerra, S., Cázares, J. M., & Olvera, M. de la L. (2010). Physical and sensing properties of ZnO:F:Al thin films deposited by sol–gel. *Thin Solid Films*, *518*(7), 1815–1820. https://doi.org/10.1016/j.tsf.2009.09.039

Mandal, S., Goswami, M. L. N., Das, K., Dhar, A., & Ray, S. K. (2008). Temperature dependent photoluminescence characteristics of nanocrystalline ZnO films grown by sol–gel technique. *Thin Solid Films*, *516*(23), 8702–8706. https://doi.org/10.1016/j.tsf.2008.05.016

Matsuda, A., & Kawamura, G. (2016). Sol–Gel Nano-/Micropatterning Process. In L. Klein, M. Aparicio, & A. Jitianu (Eds.), *Handbook of Sol-Gel Science and Technology* (pp. 1–28). Springer International Publishing. https://doi.org/10.1007/978-3-319-19454-7_81-1

Mironyuk, I., Mykytyn, I., Vasylyeva, H., & Savka, K. (2020). Sodium-modified mesoporous TiO2: Sol-gel synthesis, characterization and adsorption activity toward heavy metal cations. *Journal of Molecular Liquids*, *316*, 113840. https://doi.org/10.1016/j.molliq.2020.113840

Mosa, J., & Aparicio, M. (2020). Sol-Gel Synthesis of Nanocrystalline Mesoporous Li4Ti5O12 Thin-Films as Anodes for Li-Ion Microbatteries. *Nanomaterials*, *10*(7), 1369. https://doi.org/10.3390/nano10071369

Muchuweni, E., Sathiaraj, T. S., & Nyakotyo, H. (2017). Synthesis and characterization of zinc oxide thin films for optoelectronic applications. *Heliyon*, *3*(4), e00285. https://doi.org/10.1016/j.heliyon.2017.e00285

Nbelayim, P., Ashida, Y., Maegawa, K., Kawamura, G., Muto, H., & Matsuda, A. (2020). Preparation and Characterization of Stable and Active Pt@TiO $_2$ Core–Shell Nanoparticles as Electrocatalyst for Application in PEMFCs. *ACS Applied Energy Materials*, *3*(4), 3269–3281. https://doi.org/10.1021/acsaem.9b02169

Nbelayim, P., Kawamura, G., Abdel-Galeil, M. M., Tan, W. K., Wei, X., Muto, H., & Matsuda, A. (2018). Effects of multi-sized and -shaped Ag@TiO_2 nanoparticles on the performance of plasmonic dye-sensitized solar cells. *Journal of the Ceramic Society of Japan*, *126*(3), 139–151. https://doi.org/10.2109/jcersj2.17203

Nbelayim, P., Kawamura, G., Kian Tan, W., Muto, H., & Matsuda, A. (2017). Systematic characterization of the effect of Ag@TiO2 nanoparticles on the performance of plasmonic dye-sensitized solar cells. *Scientific Reports*, *7*(1), 15690. https://doi.org/10.1038/s41598-017-15541-z

Nisticò, R., Scalarone, D., & Magnacca, G. (2017). Sol-gel chemistry, templating and spin-coating deposition: A combined approach to control in a simple way the porosity of inorganic thin films/coatings. *Microporous and Mesoporous Materials*, *248*, 18–29. https://doi.org/10.1016/j.micromeso.2017.04.017

Prasada Rao, T., Santhosh Kumar, M. C., Safarulla, A., Ganesan, V., Barman, S. R., & Sanjeeviraja, C. (2010). Physical properties of ZnO thin films deposited at various substrate temperatures using spray pyrolysis. *Physica B: Condensed Matter*, *405*(9), 2226–2231. https://doi.org/10.1016/j.physb.2010.02.016

Qin, H., Guo, W., Huang, X., Gao, P., & Xiao, H. (2020). Preparation of yttria-stabilized ZrO2 nanofiltration membrane by reverse micelles-mediated sol-gel process and its application in pesticide wastewater treatment. *Journal of the European Ceramic Society*, *40*(1), 145–154. https://doi.org/10.1016/j.jeurceramsoc.2019.09.023

Raoufi, D., & Raoufi, T. (2009). The effect of heat treatment on the physical properties of sol–gel derived ZnO thin films. *Applied Surface Science*, *255*(11), 5812–5817. https://doi.org/10.1016/j.apsusc.2009.01.010

Rwenyagila, E. R., Agyei-Tuffour, B., Zebaze Kana, M. G., Akin-Ojo, O., & Soboyejo, W. O. (2014). Optical properties of ZnO/Al/ZnO multilayer films for large area transparent electrodes. *Journal of Materials Research*, *29*(24), 2912–2920. https://doi.org/10.1557/jmr.2014.298

Sakka, S. (2018). Sol-Gel Formation of Bulk Glasses. In L. Klein, M. Aparicio, & A. Jitianu (Eds.), *Handbook of Sol-Gel Science and Technology* (pp. 233–256). Springer International Publishing. https://doi.org/10.1007/978-3-319-32101-1_6

Shi, S., Xu, C., Wang, X., Xie, Y., Wang, Y., Dong, Q., Zhu, L., Zhang, G., & Xu, D. (2020). Electrospinning fabrication of flexible Fe3O4 fibers by sol-gel method with high saturation magnetization for heavy metal adsorption. *Materials & Design*, *186*, 108298. https://doi.org/10.1016/j.matdes.2019.108298

Sivaramakrishnan, K., & Alford, T. L. (2010). Conduction and transmission analysis in gold nanolayers embedded in zinc oxide for flexible electronics. *Applied Physics Letters*, *96*(20), 201109. https://doi.org/10.1063/1.3435467

Soo, M. T., Kawamura, G., Muto, H., Matsuda, A., Lockman, Z., & Cheong, K. Y. (2013a). Design of hierarchically meso–macroporous tetragonal ZrO2 thin films with tunable thickness by spin-coating via sol–gel template route. *Microporous and Mesoporous Materials*, *167*, 198–206. https://doi.org/10.1016/j.micromeso.2012.09.010

Soo, M. T., Kawamura, G., Muto, H., Matsuda, A., Lockman, Z., & Cheong, K. Y. (2013b). Fabrication of well-crystallized mesoporous ZrO2 thin films via Pluronic P123 templated sol–gel route. *Ceramics International*, *39*, S437–S440. https://doi.org/10.1016/j.ceramint.2012.10.109

Suwanboon, S., Tanattha, R., & Tanakorn, R. (2008). Fabrication and properties of nanocrystalline zinc oxide thin film prepared by sol-gel method. *Songklanakarin Journal of Science and Technology*, *30*(1), 65–69.

Tadanaga, K., Fujii, T., Matsuda, A., Minami, T., & Tatsumisago, M. (2004). Micropatterning of Sol-Gel Derived Thin Films Using Hydrophobic-Hydrophilic Patterned Surface. *Journal of Sol-Gel Science and Technology*, *31*(1–3), 299–302. https://doi.org/10.1023/B:JSST.0000048007.43110.fa

Takahashi, M. (2018). Responsive and Adaptive Micro Wrinkles on Organic-Inorganic Hybrid Materials. *The Chemical Record*, *18*(7–8), 1222–1231. https://doi.org/10.1002/tcr.201800007

Takahashi, M., Suzuki, K., Tokudome, Y., Malfatti, L., & Innocenzi, P. (2014). Responsive microstructures on organic–inorganic hybrid films. *Journal of Sol-Gel Science and Technology*, *70*(2), 272–277. https://doi.org/10.1007/s10971-014-3301-0

Tan, W. K., Ito, T., Kawamura, G., Muto, H., Lockman, Z., & Matsuda, A. (2017). Controlled facile fabrication of plasmonic enhanced Au-decorated ZnO nanowire arrays dye-sensitized solar cells. *Materials Today Communications*, *13*, 354–358. https://doi.org/10.1016/j.mtcomm.2017.11.004

Tan, W. K., Muto, H., Ito, T., Kawamura, G., Lockman, Z., & Matsuda, A. (2020). Facile Fabrication of Plasmonic Enhanced Noble-Metal-Decorated ZnO Nanowire Arrays for Dye-Sensitized Solar Cells. *Journal of Nanoscience and Nanotechnology*, *20*(1), 359–366. https://doi.org/10.1166/jnn.2020.17223

Tan, W. K., Muto, H., Kawamura, G., Lockman, Z., & Matsuda, A. (2021). Nanomaterial Fabrication through the Modification of Sol–Gel Derived Coatings. *Nanomaterials*, *11*(1), 181. https://doi.org/10.3390/nano11010181

Tawa, S., Sato, Y., Orikasa, Y., Matsumoto, K., & Hagiwara, R. (2019). Lithium fluoride/iron difluoride composite prepared by a fluorolytic sol–gel method: Its electrochemical behavior and charge–

discharge mechanism as a cathode material for lithium secondary batteries. *Journal of Power Sources*, *412*, 180–188. https://doi.org/10.1016/j.jpowsour.2018.11.046

Toe, M. Z., Pung, S. Y., Yaacob, K. A., Matsuda, A., Tan, W. K., & Han, S. S. (2020). Effect of TiO2 sol on the conversion efficiency of TiO2 based dye-sensitized solar cell. *Journal of Sol-Gel Science and Technology*, *95*(2), 439–446. https://doi.org/10.1007/s10971-020-05325-9

Torres Delgado, G., Zúñiga Romero, C. I., Mayén Hernández, S. A., Castanedo Pérez, R., & Zelaya Angel, O. (2009). Optical and structural properties of the sol–gel-prepared ZnO thin films and their effect on the photocatalytic activity. *Solar Energy Materials and Solar Cells*, *93*(1), 55–59. https://doi.org/10.1016/j.solmat.2008.03.020

Valverde-Aguilar, G., & Manríquez Zepeda, J. L. (2015). Photoluminescence and photoconductivity studies on amorphous and crystalline ZnO thin films obtained by sol–gel method. *Applied Physics A*, *118*(4), 1305–1313. https://doi.org/10.1007/s00339-014-8836-y

Xu, L., Shi, L., & Li, X. (2009). Preparation of nanocone ZnO thin film and its aging effect of photoluminescence. *Applied Surface Science*, *255*(11), 5957–5960. https://doi.org/10.1016/j.apsusc.2009.01.044

Zou, G., Chen, W., Liu, R., & Xu, Z. (2007). Orientation enhancement of polycrystalline ZnO thin films through thermal oxidation of electrodeposited zinc metal. *Materials Letters*, *61*(21), 4305–4308. https://doi.org/10.1016/j.matlet.2007.01.092

Formatted: Line spacing: Multiple 1,15 li

Jurnal Penelitian dan Pengkajian Ilmu Pendidikan: e-Saintika
https://journal-center.litpam.com/index.php/e-Saintika/index

July 2021 Vol. 5, No. 2
e-ISSN: 2615-6881
pp. 182-194

Synthesis and Characterization of ZnO Thin Layers using Sol-Gel Spin Coating Method

[1]Sukainil Ahzan, [2]Darminto, [3]Ferry Anggoro Ardy Nugroho, [*1]Saiful Prayogi
[1]Faculty of Applied Science and Engineering, Universitas Pendidikan Mandalika, Jl. Pemuda No. 59A, Mataram 83126, Indonesia.
[2]Faculty of Mathematics and Science, Institut Teknologi Sepuluh Nopember (ITS), Jl. Raya ITS, Surabaya 60111, Indonesia.
[2]Departmet of Physics and Astronomy, Vrije Universiteit Amsterdam, De Boelelaan 1081, 1081 HV Amsterdam, The Netherlands.

*Corresponding Author e-mail: saifulprayogi@ikipmataram.ac.id

Received: May 2021; Revised: June 2021; Published: July 2021

Abstract

The potential of thin layer in many applications has led to research on the development of many new materials and their fabrication methods. This study aimed to synthesize a thin layer of ZnO using the facile and low-cost sol-gel spin coating method. The ZnO thin layer is deposited on a glass substrate and analyzed to observe the influence of the deposition variables such as heating and rotation speed, and its aging. The characterization methods include the identification of the formed phase using X-Ray Diffractometer (XRD), and the microstructure and elemental composition using Scanning Electron Microscopy (SEM) coupled with EDS (Energy Dispersive Spectrometer). The study shows that a thin layer of ZnO is successfully deposited on a glass substrate by heat treatment at temperatures of 300 ^{o}C and 500 ^{o}C. Furthermore, XRD reveals that higher heating temperatures result in higher diffraction peak intensity. At a heating temperature of 300 °C crystals are formed but are not yet perfectly oriented, while they are at 500 °C. On the other hand, higher spin coating rotation speed gives rise to lower intensity of diffraction peak. The ZnO crystallization is easier to form in the coating process with a lower rotation (1500 rpm). Interestingly, the thin layer is stable over time where there is no significant change in each sample, both in terms of intensity and width of the ZnO crystal peak. The results indicate that gel precursor aged less than two days can form ZnO crystals. Finally, SEM results show that the surface morphology of the ZnO layer heated at 500 ^{o}C has an average grain size of 300 nm. Based on the cross-sectional results of SEM shows that the higher the coating rotation speed has resulted the thinner of the ZnO layer, where the thickness of the resulting layer is on order >5 μm.

Keywords: synthesis; characterization; ZnO thin layer; sol-gel spin coating

How to Cite: Ahzan, S., Darminto, D., Nugroho, F. A. A., & Prayogi, S. (2021). Synthesis and Characterization of ZnO Thin Layers using Sol-Gel Spin Coating Method. *Jurnal Penelitian Dan Pengkajian Ilmu Pendidikan: E-Saintika*, *5*(2), 182-194. https://doi.org/10.36312/esaintika.v5i2.506

https://doi.org/10.36312/esaintika.v5i2.506

INTRODUCTION

In recent decades, as the demand for energy continues to increase, there has been tremendous interest in developing renewable energy sources and environmentally friendly technological device systems (Matsuda & Kawamura, 2016), some of which include fuel-cells, solar-cells, supercapacitors, and efficient batteries (Tan et al., 2021). In accordance with the interest in many fields of application, thin layers of several materials have been developed by the sol-gel method (Soo et al., 2013a, 2013b). Since

being introduced by Groove in 1852, thin layer technology has undergone many developments in terms of manufacturing methods, materials used, and applications (Greene, 2017). In the thin layer processing technique, the material commonly used is metal (Jittiarporn et al., 2017; Mironyuk et al., 2020; Shi et al., 2020; Tan et al., 2020), organic, inorganic, and hybrid organic-inorganic (Kawamura et al., 2010; Nisticò et al., 2017; Takahashi, 2018; Takahashi et al., 2014).

The advancement of thin films by the sol-gel method for various applications is highly dependent on the material used. In fuel-cell applications, for example, PDDA films and microparticles of $PhSiO_{3/2}$ succeeded in increasing proton conductivity to achieve a stable proton supply (Daiko et al., 2008). Likewise, Pt/TiO_2 was demonstrated as an electrocatalyst for fuel-cell electrolyte membrane applications (Nbelayim et al., 2020). The performance of a lightweight, high-capacity battery is developed from the synthesis of Li/Ti double alkoxides in a $Li_4Ti_5O_{12}$ thin film (Mosa & Aparicio, 2020), and LiF/FeF_2 in the form of $Li0.5FeF_3$ (Kim et al., 2012; Tawa et al., 2019). Formation of superhydrophobic/superhydrophilic layers in film fabrication including surface design and film coating using Al_2O_3, ZrO_2, and TiO_2 materials (Tadanaga et al., 2004). In addition, the development of thin films by the sol-gel method is used in the extraction technology of waste disposal, especially heavy metal adsorbents , such as electro-spinned flexible Fe_3O_4 fibers (Shi et al., 2020) and yttria-stabilized ZrO_2 membranes (Qin et al., 2020). The most extensively researched is the application of thin layers as solar-cells (dye-sensitized solar cells, DSSC) (Abd-Ellah et al., 2016; Nbelayim et al., 2017, 2018, 2020; Tan et al., 2017; Toe et al., 2020), from zinc oxide material (ZnO) (Khan et al., 2017; Muchuweni et al., 2017; Prasada Rao et al., 2010).

Sol-gel coating techniques commonly used include spray coating, dip coating, roll coating, and spin coating (Tan et al., 2021). Among these, spin-coating method is the most frequently used (Khan et al., 2017). This method combines simple physical and chemical methods and has several advantages compared to other methods, for instance being cost-efficient with relatively simple setup, and excellent control over the thickness (through parameters of time, rotational speed, and viscosity of the solution) and the homogeneity of the layer (Cheng et al., 2003).

Among thin film-forming materials, zinc oxide (ZnO) is the most extensively studied because it is one of the transparent semi-conductive oxides (Zou et al., 2007) with a relatively high exciton binding energy (60 mEV) and a wide band gap around of 3.2 to 3.4 eV (Rwenyagila et al., 2014; Sivaramakrishnan & Alford, 2010; Valverde-Aguilar & Manríquez Zepeda, 2015). These advantages of optical and electrical properties allow ZnO to be applied as optical waveguides, optoelectronic devices (Çopuroğlu et al., 2009; Khan et al., 2017; Rwenyagila et al., 2014), piezoelectricity, conductive gas sensors, transparent conductive electrodes, photocatalysts and DSSC (Djurišić et al., 2010). One of the exciting properties of ZnO is its crystal formation process that occurs at temperatures under 400 ^oC. This phenomenon depends on the type of deposition and the solvent used. Previous studies showed that crystalline ZnO was formed using ethylene glycol and glycerol as a solvent at a heating temperature of 200 ^oC (Torres Delgado et al., 2009). Heating at temperatures below 300^oC is an early stage of heating, where the crystal structure has been formed but has not been oriented perfectly. Furthermore, with higher heating at 400 ^oC and 500 ^oC, the ZnO crystal structure will be perfectly oriented (Raoufi & Raoufi, 2009). Another attractive property of ZnO to observe is aging. Aging is the storage of sol-gel for a certain time

before being used as a coating material. The aging process affects the physical, electrical, and optical properties of the ZnO thin film (Xu et al., 2009).

Literature surveys reveal that reports on the properties of ZnO thin films deposited by the sol-gel technique is lacking (Khan et al., 2017). Here, we develop a thin layer of ZnO material by the sol-gel spin coating method and assess its crystallization properties and morphology. The variables that are the focus of this study include heat treatment, rotation speed, and aging

METHOD

A thin layer was deposited on a glass substrate of 5 x 10 mm^2 using a sol-gel method using zinc acetate dehydrate {$Zn(CH_3COO)_2.2H_2O$} powder (M: 219.49 g/mol, 99% Merck, Germany) with a molar ratio of 1:1 MEA:ZnAc. Ethanol (C_2H_6O) (99% technical, Merck) was used as solvent and ethanolamine (MEA: C_2H_7NO) as stabilizer, each with a purity of 99%. The solution was prepared by magnetic stirring at ±70 °C for 30 minutes. ZnAc was rather difficult to dissolve in ethanol. Therefore the dissolution process must be accompanied by heating, which was carried out on a hot plate with a temperature range of 80 to 100 °C. This was followed by the addition of MEA. After the heating process for 30 to 40 minutes, the solution was then allowed to stand at room temperature to form a gel. The gel was the divided into five parts and each was aged for 0, 10, 24, 48 and 72 hours, in air with a temperature of ±25°C and humidity of 70±5%.

The thermal behavior of ZnO gel was tested using Differential Thermal Analysis (DTA) and Thermogravimetric Analysis (TGA). This analysis aimed to observe changes in energy and mass as function of temperature. The DTA/TGA analysis results are used as a reference in determining the temperature at which the phase transformation occurs.

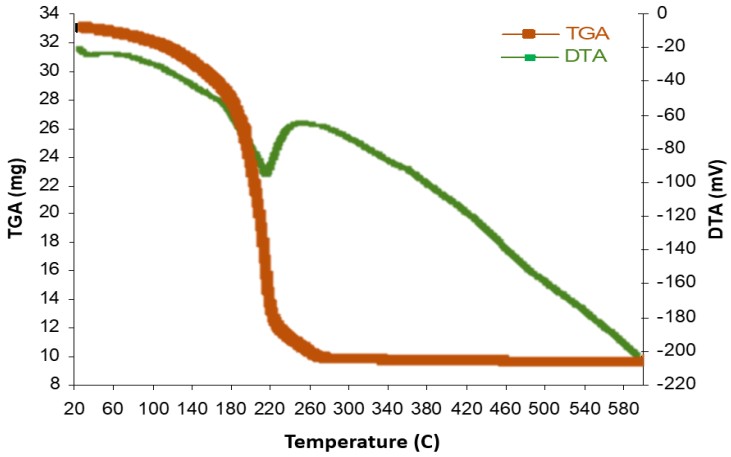

Figure 1. DTA-TGA test results of ZnO thin film deposited by spin coat sol-gel.

Based on the results of the TGA (Fig. 1), it can be seen that there is 90% decrease in mass up to a temperature of 280 °C, after which there is no further decrease in mass. This decrease in mass is followed by energy release or endothermic (DTA Graph in Fig. 1). Based on the DTA and TGA graphs, it is estimated that the change of ZnO + H_2O into ZnO crystals occurs on heating above 280 °C, so that the ZnO layer pre-heating process can be carried out at a temperature of 300 °C.

The deposition of the thin layer on a glass substrate with spin coating was also carried out at 1500, 2000, and 2500 rpm variations. A thin layer of ZnO was heated

using a furnace. The heating process was carried out in 3 stages. The first heating for 1 hour at a temperature of 100 °C (calcination) aimed to gradually remove the water content and residual solvent in the layer. The second heating at 300 °C, where the temperature was slowly increased from room temperature to 300 °C for 5 hours, was held for 6 minutes. This stage was a pre-heating stage that functioned to remove solvents from ethanol, water, MEA, and facilitated ZnOH conversion to ZnO. The next stage was post-heating or final heating at a temperature of 500 °C. Like the pre-heating process, the temperature rise was set slowly from room temperature to 500 °C in 10 hours, then held for 10 minutes. This post-heating functioned to form ZnO particles with uniform crystal orientation and eliminate the pores.

The characterization of the coating results included identification of the formed phase using X-ray Diffractometer (XRD) with the help of a search match and refinement program using Rietica software with the comparison is standard data (CPI ZnO 1011259), layer microstructure, and elemental composition observed by Scanning Electron Microscopy (SEM) coupled with EDS (Energy Dispersive Spectrometer).

RESULTS AND DISCUSSION

Effect of heating on the ZnO crystal layer

The X-ray diffraction pattern of the ZnO layer deposited at 2000 rpm at various heating temperature and aged for 24 hours is shown in Figure 2.

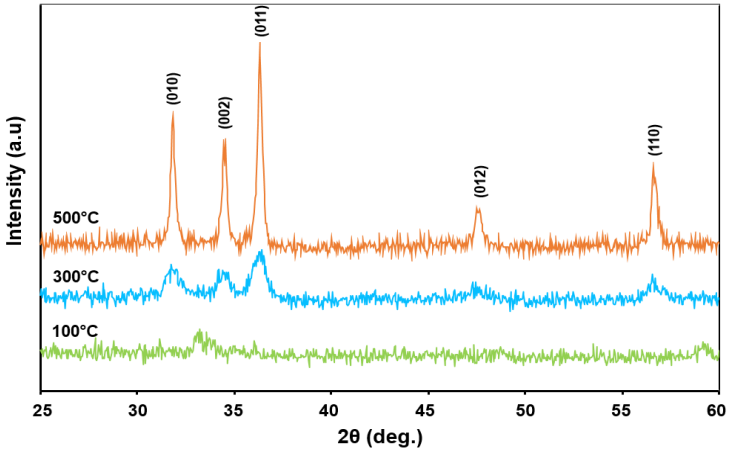

Figure 2. XRD pattern of ZnO layer with the variation of heating temperature

Based on Figure 2, it can be seen that the layer heated at a temperature of 100 °C forms two peaks at an angle of 33.15° and 59.30°. These peaks correspond to zinc propianate ($C_6H_{10}O_4Zn$) phase and zinc salicylate dihydrete {($C_6H_{10}O_6Zn$).$2H_2O$} phase, respectively. These peaks clearly originate from the solvents on the layer.

At a heating temperature of 300 °C crystals are formed but are not yet perfectly oriented. At 500 °C, the ZnO crystals are perfectly oriented. This is consistent with the results of DTA-TGA (cf. Fig. 1) in that the formation of ZnO occurs above 280 °C. With the help of the Rietica program, hexagonal ZnO has been formed with lattice parameters for a temperature of 300 °C (a = 3,245 Å, c = 5,209 Å) and a temperature of 500°C (a = 3,249 Å, c = 5,205 Å). In the range of 2θ of 25° to 60°, crystal plane peaks are formed, indicating that the layer obtained is polycrystalline.

Pre- and post-heating affect the ZnO layer in the form of solvent evaporation and reaction material decomposition. At low pre-heating temperature (< 300 °C), the (100), (002), and (101) diffraction peaks appeared with random preferential growth. This

happens because at this temperature, the reagents have completely evaporated, and the thermal decomposition of the precursors has not yet occurred. Still, they occur at post-heating temperatures above 500 °C (Suwanboon et al., 2008). The increase in the intensity of the diffraction peak at higher temperatures is due to greater energy available to increase the movement of atoms, which increases the quality and crystallization of the layer (Mandal et al., 2008).

Effect of spin coating speed on ZnO layer

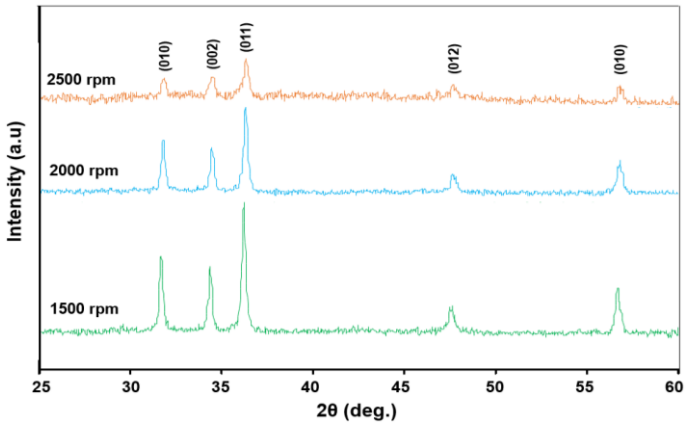

Figure 3. The XRD pattern of the ZnO layer with variations in spin coat rotational speed.

Figure 3 shows XRD results for ZnO layers made with variations in rotational speed of 1500, 2000, and 2500 rpm. The XRD peaks of the three samples show a decrease in intensity as rotation speed increases. This happens because ZnO crystallization is easier to form in the coating process with a lower rotation (1500 rpm).

Effect of aging on ZnO crystal layer

The XRD pattern of the synthesized ZnO layer with variations in aging of the precursor gel is presented in Figure 4.

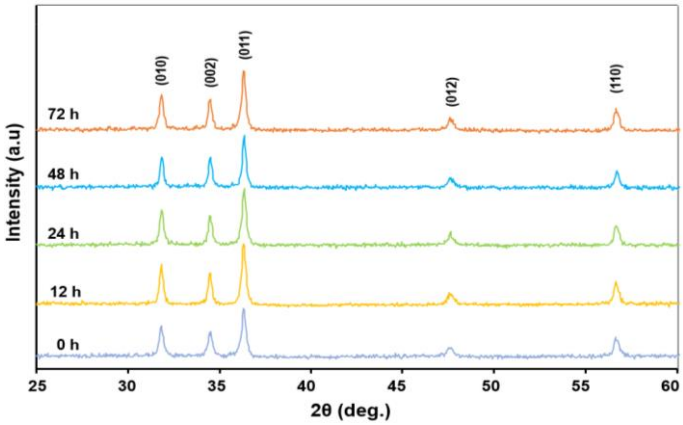

Figure 4. XRD pattern of deposited ZnO layer with an aging variation.

Based on Figure 4, there is no significant change in each sample, both in terms of intensity and width of the ZnO crystal peak. These results indicate that gel precursor aged less than two days can form ZnO crystals. The results of another study reported that after aging for seven days, the peak intensity (002) of ZnO increased compared to samples aged for up to two days (Maldonado et al., 2010). This may occur because

aging can cause further condensation of active groups and ZnO aggregation in solution and cause significant growth at peak intensity (002) of ZnO (Fathollahi & Amini, 2001).

Surface morphology of ZnO thin layer

SEM photos of the ZnO layer surface heated at 100, 300, and 500 °C, respectively, are presented in Figure 5.

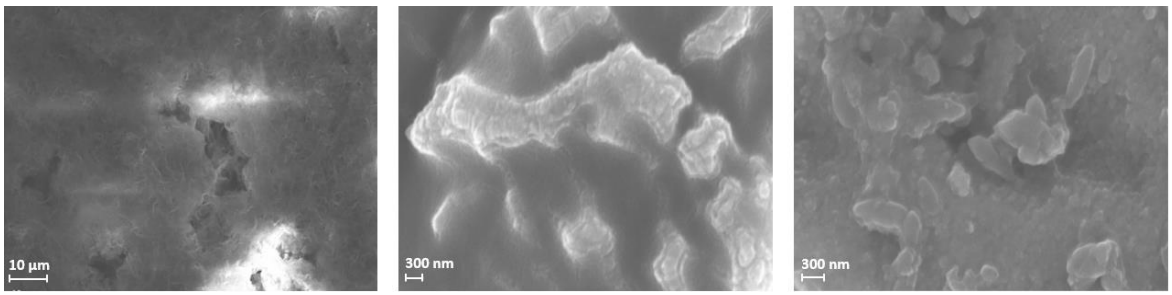

(a) (b) (c)

Figure 5. SEM photos of the ZnO layer surface heated at: (a) 100°C, (b) 300°C, and (c) 500°C.

At a temperature of 100°C (Fig. 5a), the layer is still coarse and porous, with a pore size of approximately 6–8 µm. This is because the layer still contains water molecules and solvents that have not completely evaporated at this temperature. When the layer is heated at 300 °C (pre-heating), the remaining organic matter can evaporate completely, and ZnO grains begin to grow (Fig. 5b), but the distance between the particles is still relatively large. When the ZnO layer is heated at 500 °C (Fig. 5c), the atoms in the existing grains receive sufficient driving force energy to diffuse to form new, larger grains. As a result of this inter-grain diffusion, necking will be formed, resulting in the shrinking of the boundary between grains and porosity (Fig. 5c). The average grain size at this temperature is about 300 nm.

To this end, the morphology and crystal structure of the ZnO layer made by the sol-gel process is influenced by the solvent, pre-heating and post-heating temperatures, sol concentration, substrate, and coating process (Habibi & Khaledi Sardashti, 2008). The ZnO layer's nucleation thermodynamics and crystal growth showed a transformation from an amorphous to crystalline state. The growth of crystals with the dominant c-axis orientation depends on the surface energy of the layer and the glass substrate and the interfacial energy between them. In crystal growth, the growing fields depend on the loss of slow-growing fields, with lower surface energies.

In addition to heat treatment, the morphology and thickness of the ZnO layer are also affected by the spin coating speed. Figure 6 shows the surface morphology of the coated layer at 1500, 2000, and 2500 rpm.

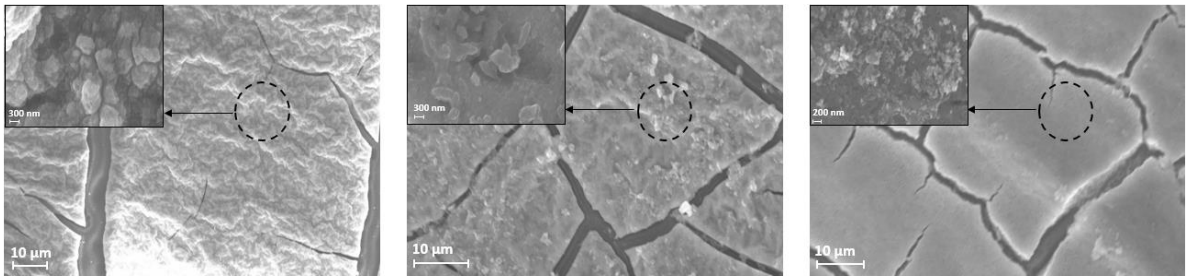

(a) (b) (c)

Figure 6. SEM photos of the ZnO layer surface coated with variations in rotation speed: (a) 1500 rpm, (b) 2000 rpm, and (c) 2500 rpm.

Based on Figure 6, it can be seen that the higher the rotation speed, the smoother the coating obtained, with smaller average grain size. The ZnO layer coated at 1500 and 2000 rpm has similar average grain size of 300 nm, while the ZnO layer coated at 2500 rpm has an average grain size of 100 nm. The results are consistent with previous studies that reported that the higher the rotational speed used to make the ZnO layer, the smaller of grain size produced (Ilican et al., 2008). The cross-sectional analysis of the coated ZnO layer with variations in rotational speed is presented in Figure 7.

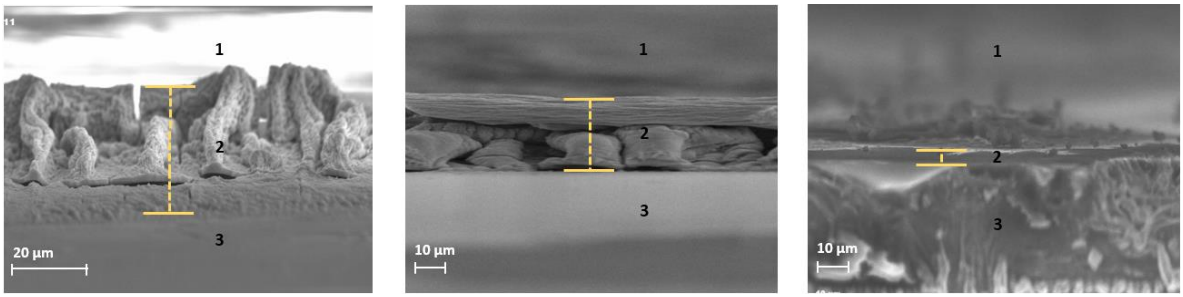

(a) (b) (c)

Figure 7. Cross-section of the coated ZnO layer with variations in rotational speed: (a) 1500 rpm, (b) 2000 rpm, and (c) 2500 rpm. (1 = air, 2 = ZnO layer thickness, 3 = substrate)

The results show that the thickness of the ZnO layer coated with 1500 rpm rotation is about 30 µm (Fig. 7a), while the layer coated with 2000 rpm rotation is about 20 µm (Fig. 7b), 2500 rpm at about 5 µm (Fig. 7c). Therefore it is confirmed that the thickness of the ZnO layer gets thinner as the rotation speed increases. In forming a coating on the substrate, it takes a large enough centrifugal speed to distribute the gel over the entire surface and remove the excess gel to the outside of the substrate. If the rotational speed is increased, the previously attached gel will be thrown out of the substrate, and the layer will thin out, or it can also disappear. This is because the binding force between the substrate and the gel is not strong enough to withstand the centrifugal force, which is too high. So, the faster the coating rotation, the more gel will leave the substrate so that the resulting layer is thinner.

From the results in Figure 6, although the layer looks smooth, most of the areas in the layer have many micron-sized cracks. These cracks are caused by the uneven heating rate on the surface of the coating layer and the different thermal coefficient between the substrate and the coating layer. Cracks also occur in the area between the

layer and the substrate (Fig. 6). Based on the cross-sectional photo of the ZnO layer (Fig. 7), it can be seen that the layer is not completely attached to the substrate. This condition makes the coating to peel off easily when exposed to scratches or friction from the outside. Cracks can also be seen from the EDX results (see Fig. 8). From the Figure we also see existence of Ca (0.98% wt) in the cracks, that originates from the substrate (from XRF results). Although the Ca content is small, this still indicates that the cracks are intense they penetrate the ZnO layer. Based on the Figure 8, it is estimated that the thickness of the ZnO layer formed with heating at 500 °C is about 5 μm to 20 μm.

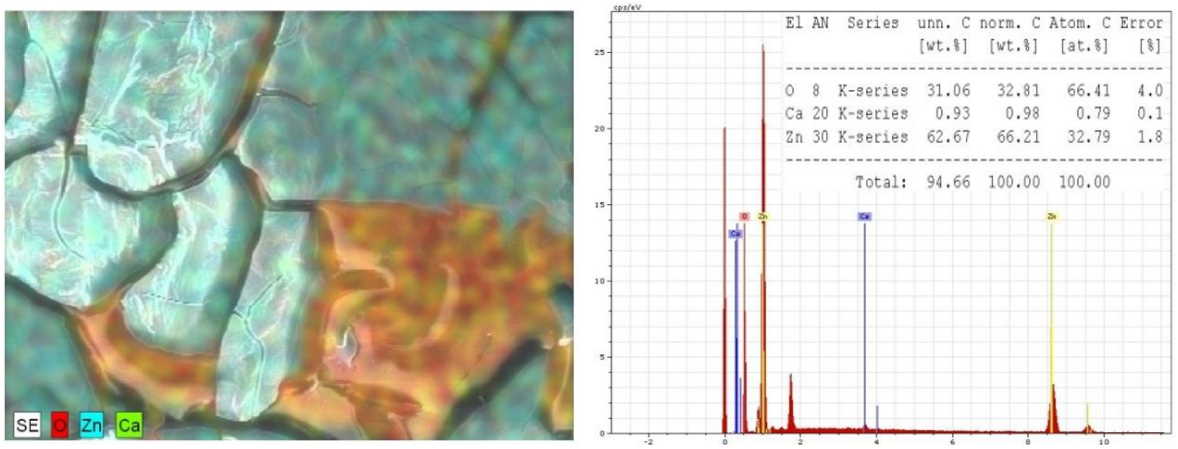

(a) (b)

Figure 8. EDX results of ZnO layer on a glass substrate: (a) surface topography, and (b) elemental content.

Microcracks may occur on the ceramic coating surface with the cracks spreading along the grain boundaries (Sakka, 2018). This phenomena happens because the layer and the substrate have a huge difference in the coefficient of thermal expansion. The spread of microcracks along the grain boundaries is formed before the crystallization process. These microcracks can be prevented by equalizing the coefficient of thermal expansion (α) between the coating and the substrate. For example BaTiO3 (α =140 x 10^{-7} K^{-1}), the layer has microcracks when deposited on a SiO2 glass substrate (α = 5 x 10^{-7} K^{-1}), but BaTiO3 has no microcracks on a single crystal substrate of MgO (α = 135 x 10^{-7} K^{-1}) (Sakka, 2018). Microcracks can occur during the heating process at low temperatures (100°C - 400°C). In another study (Kozuka & Hirano, 2000) reported that in the production of the titania layer, the crystal structure appears at a temperature of 500°C, while cracks appear at temperatures below it. This means that the crack occurs before the crystallization process.

Microcracks can also occur due to variations in the thickness of the gel layer. In the titania layer made with variations in thickness, the thicker layer is obtained, which tends to crack at low temperatures (Kozuka & Hirano, 2000). This happens because the thickness affects the occurrence of intrinsic stress during the heating process. The crack formation also depends on the heating rate. Cracks appear at higher temperatures when the coating is heated at a low heating rate. At low heating, the rate will produce a smaller porosity. This indicates that the low heating rate allows sufficient time for the coating to solidify during heating resulting in high tensile stresses in the substrate plane.

CONCLUSION

The ZnO layer was successfully deposited on a glass substrate by heat treatment at 300 °C and 500 °C. At a heating temperature of 100°C, the ZnO structure has not yet been formed, and when the heating temperature is 300 °C, crystals have started to form but have not been oriented perfectly. ZnO crystals are perfectly oriented at 500 °C. XRD results show that the higher heating temperature has resulted in higher diffraction peak intensity. At a heating temperature of 300 °C crystals are formed but are not yet perfectly oriented while at 500 °C they are. On the other hand, higher spin coating rotation speed gives rise to lower intensity of diffraction peak. The ZnO crystallization is easier to form in the coating process with a lower rotation (1500 rpm). Interestingly, the thin layer is stable over time where there is no significant change in each sample, both in terms of intensity and width of the ZnO crystal peak. The results indicate that gel precursor aged less than two days can form ZnO crystals. SEM results show that the surface morphology of the ZnO layer heated at 500 °C has an average grain size of 300 nm. The cross-sectional results of SEM show that the higher the rotation speed, the thinner the resulting ZnO layer, where the thickness of the resulting layer is on the order of > 5 μm.

RECOMMENDATION

The XRD results of the ZnO layer deposited on the glass substrate were all polycrystalline in structure. Efforts to make ZnO layer single crystal must be continued, by proper selection of substrate and higher post-heating. In addition, the SEM results show that the surface morphology of the ZnO layer is not homogeneous, there are many cracks and the size is still thick. For this reason, it is necessary to carry out more in-depth experiments in terms of the use of appropriate concentrations, speeds, and rotation times, as well as the selection of a substrate that has a heat capacity and plane orientation in accordance with the ZnO layer, for example alumina ceramic material.

ACKNOWLEDGMENT

This research received no specific grant from any funding agency in the public, commercial, or not for profit sectors.

REFERENCES

Abd-Ellah, M., Moghimi, N., Zhang, L., Thomas, Joseph. P., McGillivray, D., Srivastava, S., & Leung, K. T. (2016). Plasmonic gold nanoparticles for ZnO-nanotube photoanodes in dye-sensitized solar cell application. *Nanoscale*, *8*(3), 1658–1664. https://doi.org/10.1039/C5NR08029K

Cheng, Z., Zhang, J., & Kronmüller, H. (2003). Magnetically soft phase in magnetization reversal processes of nanocomposite Sm 2 Fe 15 Ga 2 C x / α − Fe permanent magnetic materials. *Physical Review B*, *68*(14), 144417. https://doi.org/10.1103/PhysRevB.68.144417

Çopuroğlu, M., Koh, L. H. K., O'Brien, S., & Crean, G. M. (2009). Comparative characterisation of zinc oxide thin films prepared from zinc acetate with or without water of hydration via the sol–gel method. *Journal of Sol-Gel Science and Technology*, *52*(3), 432–438. https://doi.org/10.1007/s10971-009-2016-0

Daiko, Y., Sakamoto, H., Katagiri, K., Muto, H., Sakai, M., & Matsuda, A. (2008). Deposition of Ultrathin Nafion Layers on Sol–Gel-Derived Phenylsilsesquioxane

Particles via Layer-by-Layer Assembly. *Journal of The Electrochemical Society*, *155*(5), B479. https://doi.org/10.1149/1.2885101

Djurišić, A. B., Ng, A. M. C., & Chen, X. Y. (2010). ZnO nanostructures for optoelectronics: Material properties and device applications. *Progress in Quantum Electronics*, *34*(4), 191–259. https://doi.org/10.1016/j.pquantelec.2010.04.001

Fathollahi, V., & Amini, M. M. (2001). Sol–gel preparation of highly oriented gallium-doped zinc oxide thin films. *Materials Letters*, *50*(4), 235–239. https://doi.org/10.1016/S0167-577X(01)00231-2

Greene, J. E. (2017). Review Article: Tracing the recorded history of thin-film sputter deposition: From the 1800s to 2017. *Journal of Vacuum Science & Technology A: Vacuum, Surfaces, and Films*, *35*(5), 05C204. https://doi.org/10.1116/1.4998940

Habibi, M. H., & Khaledi Sardashti, M. (2008). Structure and morphology of nanostructured zinc oxide thin films Prepared by dip-vs. Spin-coating methods. *Journal of the Iranian Chemical Society*, *5*(4), 603–609. https://doi.org/10.1007/BF03246140

Ilican, S., Caglar, Y., & Caglar, M. (2008). Preparation and Characterization Of ZnO Thin Films Deposited By Sol-Gel Spin Coating Method. *Journal of Optoelectronics and Advanced Materials*, *10*(10), 2578–2583.

Jittiarporn, P., Badilescu, S., Al Sawafta, M. N., Sikong, L., & Truong, V.-V. (2017). Electrochromic properties of sol–gel prepared hybrid transition metal oxides – A short review. *Journal of Science: Advanced Materials and Devices*, *2*(3), 286–300. https://doi.org/10.1016/j.jsamd.2017.08.005

Kawamura, G., Sato, S., Muto, H., Sakai, M., Lim, P. B., Watanabe, K., Inoue, M., & Matsuda, A. (2010). AgBr nanocrystal-dispersed silsesquioxane–titania hybrid films for holographic materials. *Materials Letters*, *64*(23), 2648–2651. https://doi.org/10.1016/j.matlet.2010.08.068

Khan, M. I., Bhatti, K. A., Qindeel, R., Alonizan, N., & Althobaiti, H. S. (2017). Characterizations of multilayer ZnO thin films deposited by sol-gel spin coating technique. *Results in Physics*, *7*, 651–655. https://doi.org/10.1016/j.rinp.2016.12.029

Kim, S. W., Nam, K. W., Seo, D. H., Hong, J., Kim, K., Gwon, H., & Kang, K. (2012). Energy storage in composites of a redox couple host and a lithium ion host. *Nano Today*, *7*(3), 168–173. https://doi.org/10.1016/j.nantod.2012.04.004

Kozuka, H., & Hirano, M. (2000). Radiative Striations and Surface Roughness of Alkoxide-Derived Spin Coating Films. *Journal of Sol-Gel Science and Technology*, *19*(1/3), 501–504. https://doi.org/10.1023/A:1008772102546

Maldonado, A., Tirado-Guerra, S., Cázares, J. M., & Olvera, M. de la L. (2010). Physical and sensing properties of ZnO:F:Al thin films deposited by sol–gel. *Thin Solid Films*, *518*(7), 1815–1820. https://doi.org/10.1016/j.tsf.2009.09.039

Mandal, S., Goswami, M. L. N., Das, K., Dhar, A., & Ray, S. K. (2008). Temperature dependent photoluminescence characteristics of nanocrystalline ZnO films grown by sol–gel technique. *Thin Solid Films*, *516*(23), 8702–8706. https://doi.org/10.1016/j.tsf.2008.05.016

Matsuda, A., & Kawamura, G. (2016). Sol–Gel Nano-/Micropatterning Process. In L. Klein, M. Aparicio, & A. Jitianu (Eds.), *Handbook of Sol-Gel Science and Technology* (pp. 1–28). Springer International Publishing. https://doi.org/10.1007/978-3-319-19454-7_81-1

Mironyuk, I., Mykytyn, I., Vasylyeva, H., & Savka, K. (2020). Sodium-modified mesoporous TiO2: Sol-gel synthesis, characterization and adsorption activity toward heavy metal cations. *Journal of Molecular Liquids*, *316*, 113840. https://doi.org/10.1016/j.molliq.2020.113840

Mosa, J., & Aparicio, M. (2020). Sol-Gel Synthesis of Nanocrystalline Mesoporous Li4Ti5O12 Thin-Films as Anodes for Li-Ion Microbatteries. *Nanomaterials*, *10*(7), 1369. https://doi.org/10.3390/nano10071369

Muchuweni, E., Sathiaraj, T. S., & Nyakotyo, H. (2017). Synthesis and characterization of zinc oxide thin films for optoelectronic applications. *Heliyon*, *3*(4), e00285. https://doi.org/10.1016/j.heliyon.2017.e00285

Nbelayim, P., Ashida, Y., Maegawa, K., Kawamura, G., Muto, H., & Matsuda, A. (2020). Preparation and Characterization of Stable and Active Pt@TiO $_2$ Core–Shell Nanoparticles as Electrocatalyst for Application in PEMFCs. *ACS Applied Energy Materials*, *3*(4), 3269–3281. https://doi.org/10.1021/acsaem.9b02169

Nbelayim, P., Kawamura, G., Abdel-Galeil, M. M., Tan, W. K., Wei, X., Muto, H., & Matsuda, A. (2018). Effects of multi-sized and -shaped Ag@TiO_2 nanoparticles on the performance of plasmonic dye-sensitized solar cells. *Journal of the Ceramic Society of Japan*, *126*(3), 139–151. https://doi.org/10.2109/jcersj2.17203

Nbelayim, P., Kawamura, G., Kian Tan, W., Muto, H., & Matsuda, A. (2017). Systematic characterization of the effect of Ag@TiO2 nanoparticles on the performance of plasmonic dye-sensitized solar cells. *Scientific Reports*, *7*(1), 15690. https://doi.org/10.1038/s41598-017-15541-z

Nisticò, R., Scalarone, D., & Magnacca, G. (2017). Sol-gel chemistry, templating and spin-coating deposition: A combined approach to control in a simple way the porosity of inorganic thin films/coatings. *Microporous and Mesoporous Materials*, *248*, 18–29. https://doi.org/10.1016/j.micromeso.2017.04.017

Prasada Rao, T., Santhosh Kumar, M. C., Safarulla, A., Ganesan, V., Barman, S. R., & Sanjeeviraja, C. (2010). Physical properties of ZnO thin films deposited at various substrate temperatures using spray pyrolysis. *Physica B: Condensed Matter*, *405*(9), 2226–2231. https://doi.org/10.1016/j.physb.2010.02.016

Qin, H., Guo, W., Huang, X., Gao, P., & Xiao, H. (2020). Preparation of yttria-stabilized ZrO2 nanofiltration membrane by reverse micelles-mediated sol-gel process and its application in pesticide wastewater treatment. *Journal of the European Ceramic Society*, *40*(1), 145–154. https://doi.org/10.1016/j.jeurceramsoc.2019.09.023

Raoufi, D., & Raoufi, T. (2009). The effect of heat treatment on the physical properties of sol–gel derived ZnO thin films. *Applied Surface Science*, *255*(11), 5812–5817. https://doi.org/10.1016/j.apsusc.2009.01.010

Rwenyagila, E. R., Agyei-Tuffour, B., Zebaze Kana, M. G., Akin-Ojo, O., & Soboyejo, W. O. (2014). Optical properties of ZnO/Al/ZnO multilayer films for large area transparent electrodes. *Journal of Materials Research*, *29*(24), 2912–2920. https://doi.org/10.1557/jmr.2014.298

Sakka, S. (2018). Sol-Gel Formation of Bulk Glasses. In L. Klein, M. Aparicio, & A. Jitianu (Eds.), *Handbook of Sol-Gel Science and Technology* (pp. 233–256). Springer International Publishing. https://doi.org/10.1007/978-3-319-32101-1_6

Shi, S., Xu, C., Wang, X., Xie, Y., Wang, Y., Dong, Q., Zhu, L., Zhang, G., & Xu, D. (2020). Electrospinning fabrication of flexible Fe3O4 fibers by sol-gel method with high saturation magnetization for heavy metal adsorption. *Materials & Design*, *186*, 108298. https://doi.org/10.1016/j.matdes.2019.108298

Sivaramakrishnan, K., & Alford, T. L. (2010). Conduction and transmission analysis in gold nanolayers embedded in zinc oxide for flexible electronics. *Applied Physics Letters*, *96*(20), 201109. https://doi.org/10.1063/1.3435467

Soo, M. T., Kawamura, G., Muto, H., Matsuda, A., Lockman, Z., & Cheong, K. Y. (2013a). Design of hierarchically meso–macroporous tetragonal ZrO2 thin films with tunable thickness by spin-coating via sol–gel template route. *Microporous and Mesoporous Materials*, *167*, 198–206. https://doi.org/10.1016/j.micromeso.2012.09.010

Soo, M. T., Kawamura, G., Muto, H., Matsuda, A., Lockman, Z., & Cheong, K. Y. (2013b). Fabrication of well-crystallized mesoporous ZrO2 thin films via Pluronic P123 templated sol–gel route. *Ceramics International*, *39*, S437–S440. https://doi.org/10.1016/j.ceramint.2012.10.109

Suwanboon, S., Tanattha, R., & Tanakorn, R. (2008). Fabrication and properties of nanocrystalline zinc oxide thin film prepared by sol-gel method. *Songklanakarin Journal of Science and Technology*, *30*(1), 65–69.

Tadanaga, K., Fujii, T., Matsuda, A., Minami, T., & Tatsumisago, M. (2004). Micropatterning of Sol-Gel Derived Thin Films Using Hydrophobic-Hydrophilic Patterned Surface. *Journal of Sol-Gel Science and Technology*, *31*(1–3), 299–302. https://doi.org/10.1023/B:JSST.0000048007.43110.fa

Takahashi, M. (2018). Responsive and Adaptive Micro Wrinkles on Organic-Inorganic Hybrid Materials. *The Chemical Record*, *18*(7–8), 1222–1231. https://doi.org/10.1002/tcr.201800007

Takahashi, M., Suzuki, K., Tokudome, Y., Malfatti, L., & Innocenzi, P. (2014). Responsive microstructures on organic–inorganic hybrid films. *Journal of Sol-Gel Science and Technology*, *70*(2), 272–277. https://doi.org/10.1007/s10971-014-3301-0

Tan, W. K., Ito, T., Kawamura, G., Muto, H., Lockman, Z., & Matsuda, A. (2017). Controlled facile fabrication of plasmonic enhanced Au-decorated ZnO nanowire arrays dye-sensitized solar cells. *Materials Today Communications*, *13*, 354–358. https://doi.org/10.1016/j.mtcomm.2017.11.004

Tan, W. K., Muto, H., Ito, T., Kawamura, G., Lockman, Z., & Matsuda, A. (2020). Facile Fabrication of Plasmonic Enhanced Noble-Metal-Decorated ZnO Nanowire Arrays for Dye-Sensitized Solar Cells. *Journal of Nanoscience and Nanotechnology*, *20*(1), 359–366. https://doi.org/10.1166/jnn.2020.17223

Tan, W. K., Muto, H., Kawamura, G., Lockman, Z., & Matsuda, A. (2021). Nanomaterial Fabrication through the Modification of Sol–Gel Derived Coatings. *Nanomaterials*, *11*(1), 181. https://doi.org/10.3390/nano11010181

Tawa, S., Sato, Y., Orikasa, Y., Matsumoto, K., & Hagiwara, R. (2019). Lithium fluoride/iron difluoride composite prepared by a fluorolytic sol–gel method: Its electrochemical behavior and charge–discharge mechanism as a cathode material for lithium secondary batteries. *Journal of Power Sources*, *412*, 180–188. https://doi.org/10.1016/j.jpowsour.2018.11.046

Toe, M. Z., Pung, S. Y., Yaacob, K. A., Matsuda, A., Tan, W. K., & Han, S. S. (2020). Effect of TiO2 sol on the conversion efficiency of TiO2 based dye-sensitized solar cell. *Journal of Sol-Gel Science and Technology*, *95*(2), 439–446. https://doi.org/10.1007/s10971-020-05325-9

Torres Delgado, G., Zúñiga Romero, C. I., Mayén Hernández, S. A., Castanedo Pérez, R., & Zelaya Angel, O. (2009). Optical and structural properties of the sol–gel-

prepared ZnO thin films and their effect on the photocatalytic activity. *Solar Energy Materials and Solar Cells*, *93*(1), 55–59. https://doi.org/10.1016/j.solmat.2008.03.020

Valverde-Aguilar, G., & Manríquez Zepeda, J. L. (2015). Photoluminescence and photoconductivity studies on amorphous and crystalline ZnO thin films obtained by sol–gel method. *Applied Physics A*, *118*(4), 1305–1313. https://doi.org/10.1007/s00339-014-8836-y

Xu, L., Shi, L., & Li, X. (2009). Preparation of nanocone ZnO thin film and its aging effect of photoluminescence. *Applied Surface Science*, *255*(11), 5957–5960. https://doi.org/10.1016/j.apsusc.2009.01.044

Zou, G., Chen, W., Liu, R., & Xu, Z. (2007). Orientation enhancement of polycrystalline ZnO thin films through thermal oxidation of electrodeposited zinc metal. *Materials Letters*, *61*(21), 4305–4308. https://doi.org/10.1016/j.matlet.2007.01.092